

1 **Dissecting super-enhancer hierarchy based on chromatin interactions**

2

3 Jialiang Huang^{1,2,5}, Kailong Li^{3,5}, Wenqing Cai², Xin Liu³, Yuannyu Zhang³, Stuart H.
4 Orkin^{2,4}, Jian Xu^{3*}, Guo-Cheng Yuan^{1*}

5

6 ¹Department of Biostatistics and Computational Biology, Dana-Farber Cancer
7 Institute and Harvard T.H. Chan School of Public Health, Boston, MA 02215, USA

8 ²Division of Hematology/Oncology, Boston Children's Hospital and Department of
9 Pediatric Oncology, Dana-Farber Cancer Institute, Harvard Stem Cell Institute, Harvard
10 Medical School, Boston, MA 02215, USA.

11 ³Children's Medical Center Research Institute, Department of Pediatrics, University of
12 Texas Southwestern Medical Center, Dallas, TX 75390, USA.

13 ⁴Howard Hughes Medical Institute, Boston, MA 02215, USA.

14 ⁵These authors contributed equally to this work.

15

16 *To whom correspondence should be addressed. E-mail: Jian Xu

17 (jian.xu@utsouthwestern.edu) and Guo-Cheng Yuan (gcyuan@jimmy.harvard.edu)

18

19 **Abstract**

20 Recent studies have highlighted super-enhancers (SEs) as important regulatory
21 elements for gene expression, but their intrinsic properties remain incompletely
22 characterized. Through an integrative analysis of Hi-C and ChIP-seq data, we find that a
23 significant fraction of SEs are hierarchically organized, containing both hub and non-hub
24 enhancers. Hub enhancers share similar histone marks with non-hub enhancers, but are
25 distinctly associated with cohesin and CTCF binding sites and disease-associated
26 genetic variants. Genetic ablation of hub enhancers results in profound defects in gene
27 activation and local chromatin landscape. As such, hub enhancers are the major
28 constituents responsible for SE functional and structural organization.

29

30 **Keywords**

31 Super-enhancer, Chromatin interaction, Hub enhancer, Hierarchy, CTCF

32

33 **Introduction**

34 Enhancers are *cis*-acting DNA sequences that control cell-type specific gene
35 expression(Banerji, Rusconi, & Schaffner, 1981). Super-enhancers (SEs) are putative
36 enhancer clusters with unusually high levels of enhancer activity and enrichment of
37 enhancer-associated chromatin features including occupancy of master regulators,
38 coactivators, Mediators and chromatin factors (Hnisz et al., 2013; Parker et al., 2013;
39 Whyte et al., 2013). SEs are often in close proximity to critical cell identity-associated
40 genes, supporting a model in which a small set of lineage-defining SEs determine cell
41 identity in development and disease.

42 Despite the proposed prominent roles, the structural and functional differences
43 between SEs and regular enhancers (REs) remain poorly understood(Pott & Lieb, 2015).
44 A few SEs have been dissected by genetic manipulation of individual constituent
45 enhancers. In some studies, the results are consistent with a model whereby SEs are
46 composed of a hierarchy of both essential and dispensable constituent enhancers to
47 coordinate gene transcription(Hay et al., 2016; Hnisz et al., 2015; Huang et al., 2016; H.
48 Y. Shin et al., 2016). Due to the technical challenges in systematic characterization of
49 SEs on a larger scale, it remains difficult to evaluate the generality of hierarchical SE
50 organization in the mammalian genome.

51 Enhancer activities are mediated by the 3D chromatin interactions. Recent
52 advances in Hi-C(Lieberman-Aiden et al., 2009) and ChIA-PET(Fullwood et al., 2009)
53 technologies enable systematic interrogation of the genome-wide landscapes of
54 chromatin interactions across multiple cell types and growth conditions(Dixon et al.,
55 2015; Dixon et al., 2012; Downen et al., 2014; Javierre et al., 2016; Ji et al., 2016; Jin et
56 al., 2013; Rao et al., 2014; Tang et al., 2015). These data strongly indicate that the 3D
57 chromatin organization is highly modular, containing compartments, topologically
58 associating domains (TADs), and insulated neighborhoods. Of note, genomic loci with
59 high frequency of chromatin interactions are highly enriched for SEs(Huang, Marco,
60 Pinello, & Yuan, 2015; Schmitt et al., 2016), suggesting that proper 3D chromatin
61 configuration may be essential for orchestrating SE activities.

62 Here we developed an approach to dissect the compositional organization of
63 SEs, based on the patterns of long-range chromatin interactions. We found that a subset
64 of SEs exhibits a hierarchical structure, and hub enhancers within hierarchical SEs play
65 distinct roles in chromatin organization and gene activation. Our findings also identified a
66 critical role for CTCF in organizing the structural (and hence functional) hierarchy of SEs.

67

68 **Results**

69 **A subset of SEs contains hierarchical structure**

70 To systematically characterize the structural organization of SEs, we developed a
71 computational approach that integrates high resolution Hi-C and ChIP-seq data (**Fig.**
72 **1a**), We defined SEs with the standard ROSE algorithm(Loven et al., 2013; Whyte et al.,
73 2013). Briefly, neighboring enhancer elements defined based on H3K27ac ChIP-seq
74 peaks were merged and ranked based on the H3K27ac ChIP-seq signal, where top
75 ranked regions were designated as SEs. To quantify the degree of structural hierarchy
76 associated with each SE, we defined a computational metric, called hierarchical score
77 (or H-score for short), as follows. First, we divided each SE into 5kb bins to match the
78 resolution of Hi-C data (**Fig. 1b**). Next, we normalized the frequency of chromatin
79 interactions within each SE by transforming the raw frequency values to z-scores. Third,
80 we evaluated the maximum z-score across all bins in each SE, and referred to the
81 outcome as the H-score associated with the SE. A higher H-score value indicates the
82 chromatin interactions associated with a SE are mediated through a small subset of
83 constitutive elements (**Fig. 1b**). Fourth, by applying a threshold value of H-score, we
84 divided all SEs into two categories, which we referred as hierarchical and non-
85 hierarchical SEs, respectively (**Fig. 1b**). Finally, if an enhancer element within
86 hierarchical SEs is associated with a z-score greater than the threshold of H-score, the
87 element is referred as a hub enhancer, whereas the remaining enhancers within the
88 same SE are termed non-hub enhancers (**Fig. 1b**).

89 We applied this pipeline to dissect the SE hierarchy in two human cell lines K562
90 (erythroleukemia cells) and GM12878 (B-cell lymphoblastoid cells), using publicly
91 available high-resolution Hi-C and ChIP-seq data(T. E. P. Consortium, 2012; Rao et al.,
92 2014). In total, we identified 843 and 834 SEs in K562 and GM12878 cells, respectively.
93 On comparison of high-resolution (5kb) Hi-C profiles in K562 and GM12878 cells(Jin et
94 al., 2013), we observed that SEs contain a significantly higher frequency of chromatin
95 interactions than regular enhancers ($P = 1.2E-69$ in K562, $P = 2.0E-123$ in GM12878,
96 Student's t-test, **Supplementary Fig. 1a**), consistent with previous studies(Huang et al.,
97 2015; Schmitt et al., 2016). By applying a threshold value of H-score = 1.5, which
98 roughly corresponds to the 95th percentile of z-scores (**Supplementary Fig. 1b**), we
99 divided SEs into two categories: hierarchical and non-hierarchical SEs (**Supplementary**
100 **Fig. 1c**). As expected, hub enhancers display a higher frequency of chromatin
101 interactions than non-hub enhancers (**Supplementary Fig. 1d**). On average, both hub

102 and non-hub enhancers within SEs contain a higher frequency of chromatin interactions
103 than REs.

104 In total, we identified 215 (23% of all SEs) and 319 hierarchical SEs (34%) in
105 K562 and GM12878 cells, respectively (**Fig. 1c** and **Supplementary Fig. 2a**). The
106 hierarchical SEs tend to be ranked higher than non-hierarchical SEs based by the ROSE
107 algorithm ($P = 1.2E-25$ in K562, $P = 2.5E-21$ in GM12878, Wilcoxon rank-sum test,
108 respectively, **Fig. 1d** and **Supplementary Fig. 2b**). Using GREAT functional
109 analysis(McLean et al., 2010), we observed that, compared with non-hierarchical SEs,
110 hierarchical SEs were more enriched with gene ontology (GO) terms associated with
111 cell-type-specific biological processes, such as ‘blood coagulation’ in K562 cells and ‘B
112 cell homeostasis’ in GM12878 cells (**Fig. 1e** and **Supplementary Fig. 2c**). These results
113 suggest that hierarchical SEs may play a more important role in the maintenance of cell
114 identity.

115

116 **Both hub and non-hub enhancers are associated with active chromatin marks and** 117 **master regulators**

118 To further investigate molecular differences between hub and non-hub enhancers within
119 hierarchical SEs, we compared the spatial patterns of histone marks among three
120 enhancer groups: hub, non-hub and REs. Compared with non-hub enhancers, hub
121 enhancers display no significant difference in H3K4me1 ChIP-seq signal (**Fig. 2a** and
122 **Supplementary Fig. 3a**), but are slightly more enriched for H3K27ac and DNase I
123 hypersensitivity (**Fig. 2b,c** and **Supplementary Fig. 3b,c**).

124 One of the hallmark features of SEs is the enrichment of cell type-specific master
125 regulators and coactivators(Whyte et al., 2013). We then compared the distribution of
126 transcription factor binding profiles. Hub enhancers contain moderate but significantly
127 higher ChIP-seq signals for the binding of lineage-regulating master regulators than non-
128 hub enhancers, such as GATA1 and TAL1 in K562 cells, and PAX5 and EBF1 in
129 GM12878 cells (**Fig. 2d,e** and **Supplementary Fig. 3d,e**). Hub enhancers also display
130 increased occupancy of histone acetyltransferase p300, a coactivator associated with
131 active enhancers (**Fig. 2f** and **Supplementary Fig. 3f**). Taken together, these results
132 demonstrate that hub and non-hub enhancers are characterized by quantitative
133 differences in the occupancy of active enhancer-associated histone modifications and
134 lineage-specifying transcription factors (TFs).

135

136 **Hub enhancers are distinctively enriched with cohesin and CTCF binding**

137 Since hub and non-hub enhancers are defined based on the frequency of chromatin
138 interactions, we next compared the occupancy of cohesin and CTCF, two factors
139 essential for mediating long-range enhancer-promoter interactions and DNA looping (Ing-
140 Simmons et al., 2015). To this end, we compared the enhancer groups with the ChIP-
141 seq profiles for CTCF and two cohesin components, SMC3 and RAD21. Compared with
142 non-hub enhancers, the occupancy of all three factors is markedly elevated at hub
143 enhancers (**Fig. 3a-c** and **Supplementary Fig. 4a-c**), consistent with a critical role of
144 CTCF and cohesin in mediating chromatin interactions associated with hub enhancers.
145 Importantly, while the role of CTCF in mediating chromatin organization, such as TADs,
146 has been well established (Dixon et al., 2012), its association with SE constituents has
147 not been previously reported. In fact, only a small fraction (6% in K562; 24% in
148 GM12878) of hub enhancers overlap with known TAD boundaries (**Fig. 3d** and
149 **Supplementary Fig. 4d**), which is comparable to the genome-wide frequency of CTCF
150 peaks overlapping with TAD boundaries, suggesting a TAD-independent role of CTCF.

151 To identify potential contextual differences between CTCF binding associated
152 with distinct functions, we divided the CTCF ChIP-seq peaks into three non-overlapping
153 subsets that overlap with hub enhancers, non-hub enhancers or TAD boundaries,
154 respectively. To further distinguish CTCF binding at distinct regulatory regions, we
155 excluded peaks that overlap with both hub enhancers and TAD boundaries (**Fig. 3d** and
156 **Supplementary Fig. 4d**). We first examined the cross cell-type variability of CTCF
157 binding based on CTCF ChIP-seq signals in 55 cell types from ENCODE (T. E. P.
158 Consortium, 2012). Consistent with previous studies (Dixon et al., 2012; Pope et al.,
159 2014), we found that CTCF binding sites associated with TAD boundaries are highly
160 conserved (**Fig. 3e** and **Supplementary Fig. 4e**). In addition, within SEs, CTCF sites
161 associated with hub enhancers are more conserved than those associated with non-hub
162 enhancers. We hypothesized that the cell-type variability of CTCF binding may reflect
163 the binding affinity of CTCF to its cognate sequences, which can be quantified by the
164 motif-matching scores. Therefore, we compared the distribution of motif scores
165 associated with different subsets of CTCF binding sites. The motif scores for CTCF sites
166 associated with TAD boundaries and hub enhancers are higher than non-hub enhancer-
167 associated CTCF sites, consistent with the CTCF ChIP-seq signal intensity (**Fig. 3f** and
168 **Supplementary Fig. 4f**). Of note, a similar pattern is observed for the genomic
169 sequence conservation of CTCF binding sites as quantified by the phastCons100way

170 score (**Fig. 3g** and **Supplementary Fig. 4g**), suggesting that the cell-type variation
171 associated with CTCF binding may be under evolutionary pressure.

172 Somatic mutations of TAD or insulated neighborhood boundaries have been
173 reported in cancer(Flavahan et al., 2016; Hnisz, Weintraub, et al., 2016; Katainen et al.,
174 2015). Consistently, we observed high frequency of somatic mutations in TAD boundary-
175 associated CTCF sites using somatic mutations in different cancers from the ICGC
176 database(International Cancer Genome et al., 2010). Hub-enhancer-associated CTCF
177 sites display comparable rates of somatic mutations with TAD boundaries-associated
178 CTCF sites, which are significantly higher than non-hub enhancer-associated CTCF
179 sites ($P = 9.0E-3$ in K562, $P = 2.3E-2$ in GM12878, **Fig. 3h** and **Supplementary Fig. 4h**).
180 Our results suggest that genetic alterations of hub enhancer-associated CTCF sites may
181 confer similar consequences as perturbations of TAD boundary-associated CTCF sites,
182 such as activation of proto-oncogenes(Flavahan et al., 2016; Hnisz, Weintraub, et al.,
183 2016). Taken together, our results support a model that hub enhancers have two
184 molecularly and functionally related roles in SE hierarchy (**Fig. 3i**). Hub enhancers act as
185 ‘conventional’ enhancers to activate gene expression through the recruitment of lineage-
186 specifying transcriptional regulators and coactivators. In addition, they act as
187 ‘organizational’ hubs to mediate and/or facilitate long-range chromatin interactions
188 through the recruitment of cohesin and CTCF complexes.

189

190 **Hub enhancers are enriched for genetic variants associated with cell-type-specific** 191 **gene expression and diseases**

192 Genetic variations colocalized with regulatory genomic elements often associate with
193 variation in expression of the linked target genes. As such, expression quantitative trait
194 loci (eQTL) enrichment analysis serves as an objective and quantitative metric to
195 evaluate regulatory potential. We compared the frequencies of eQTLs that are
196 significantly associated with gene expression from the GTEx eQTL database(G. T.
197 Consortium, 2013) with hub, non-hub and regular enhancers (**Fig. 4a** and
198 **Supplementary Fig. 5a**). We observed that SEs are more enriched with eQTLs than
199 regular enhancers (**Supplementary Fig. 6a**). Importantly, within SEs, hub enhancers
200 are more enriched with eQTLs compared to non-hub enhancers (**Fig. 4a** and
201 **Supplementary Fig. 5a**). The difference is more apparent in the comparison using
202 eQTLs identified in blood cells (**Fig. 4b,c** and **Supplementary Fig. 5b,c**).

203 To gain insights into the function of hub enhancers, we next compared the
204 enhancer groups with genome-wide association study (GWAS)-identified disease-
205 associated genetic variants. Specifically, we analyzed the enrichment of single-
206 nucleotide polymorphisms (SNPs) linked to diverse phenotypic traits and diseases in the
207 GWAS catalog (Welter et al., 2014). Whereas REs are 1.6- and 1.9-fold more enriched
208 with GWAS SNPs relative to genome background in K562 and GM12878 cells,
209 respectively, the enrichment scores for SEs are significantly higher (2.7- and 4.8-fold,
210 respectively) (**Supplementary Fig. 6a**). The enrichment of GWAS SNPs at SEs is
211 consistent with previous studies that SEs are enriched with disease-associated
212 variants (Hnisz et al., 2013; Maurano et al., 2012). Importantly, within SEs, hub
213 enhancers display significantly higher enrichment (6.4- and 6.8-fold) than non-hub
214 enhancers (2.5- and 4.5-fold) or REs (**Fig. 4d** and **Supplementary Figure 5d**).
215 Furthermore, hub enhancers in K562 cells display the highest enrichment of GWAS
216 SNPs associated with blood traits (22.4-fold, **Fig. 4e,f**), indicating that hub enhancers
217 enrich for cell-type-specific diseases-associated variants. We also found the hub
218 enhancers defined by different thresholds of H-scores display similar enrichment of
219 eQTLs and GWAS SNPs (**Supplementary Fig. 6b,c**), indicating that the properties of
220 hub enhancers are not dependent on the specific threshold of H-score. Taken together,
221 our studies demonstrate that hub enhancers within SEs are most significantly enriched
222 with genetic variants associated with diseases and cell-type-specific gene expression,
223 supporting their roles in the control of cell identity and disease.

224 To test the robustness of our method, we repeated our analysis to define
225 hierarchical SEs and hub enhancers based on CTCF-mediated ChIA-PET datasets in
226 K562 and GM12878 cells (Tang et al., 2015) (see Methods). We observed that 102 of
227 188 hierarchical SEs in K562 and 227 of 427 hierarchical SEs in GM12878 defined by
228 ChIA-PET datasets overlap with those defined by Hi-C data ($P < 2.2E-16$ in both K562
229 and GM12878, Fisher's exact test, **Supplementary Fig. 7a**). The hub enhancers within
230 the hierarchical SEs shared by both data types also significantly overlap ($P < 2.2E-16$
231 in both K562 and GM12878, Fisher's exact test). Similar to previous analysis, we
232 observed that hub enhancers defined by ChIA-PET data were also more enriched with
233 disease-associated variants compared to non-hub enhancers (**Supplementary Fig. 7b**).
234 The consistency between analyzing two independent experimental platforms (Hi-C and
235 ChIA-PET), as well as between analyzing two distinct cell types (K562 and GM12878),
236 strongly indicates that our approach is robust and generally applicable.

237

238 ***In situ* genome editing reveals distinct requirement of hub vs non-hub enhancers**
239 **in SE function**

240 Since the structural organization of chromatin plays a critical role in establishing
241 enhancer activities, we then compared the regulatory potential of hub and non-hub
242 enhancers subjected to genetic perturbation. In prior work, we applied CRISPR/Cas9
243 based genome-editing to systematically dissect the functional hierarchy of an erythroid-
244 specific SE controlling the *SLC25A37* gene encoding the mitochondrial transporter
245 critical for iron metabolism(Huang et al., 2016). Following deletion of each of the three
246 constituent enhancers alone or in combination, we identified a functionally ‘dominant’
247 enhancer responsible for the vast majority of enhancer activity(Huang et al., 2016). Of
248 note, we found that this ‘dominant’ enhancer is identified as a hub enhancer and
249 associated with significantly higher chromatin interactions compared to the neighboring
250 non-hub enhancers (**Supplementary Fig. 8a**). These studies provide initial evidence
251 that hub enhancers may be more transcriptionally potent than non-hub enhancers in
252 gene activation.

253 To further establish the functional roles of hub enhancers, we performed
254 experimental validation of hierarchical SEs identified in K562 cells based on the
255 predictions of our model. We first employed CRISPR interference (CRISPRi) in which
256 the nuclease-dead Cas9 protein (dCas9) is fused to a KRAB (Kruppel-associated box)
257 transcriptional repressor domain(Gilbert et al., 2014; Thakore et al., 2015). Upon co-
258 expression of sequence-specific single guide RNAs (sgRNAs) targeting individual hub or
259 non-hub enhancers in K562 cells, we measured the expression of SE-linked target
260 genes as a readout for the functional requirement for SE activity. We focused on two
261 representative SE clusters located in the proximity of the *MYO1D* and *SMYD3* genes
262 (**Supplementary Fig. 8b,c** and **Fig. 6a,b**). Both SEs were predicted to contain
263 hierarchical structure (H-score=2.2 and 1.6 respectively), while their nearest target
264 genes *MYO1D* and *SMYD3* are highly expressed in K562 cells. Moreover, both SEs
265 contain hub and non-hub enhancers within a defined TAD domain (**Supplementary Fig.**
266 **8b,c**). Importantly, whereas CRISPRi-mediated repression of the two non-hub
267 enhancers at the *MYO1D* SE led to modest downregulation (3.1-fold) of *MYO1D*
268 expression, repression of the hub enhancer significantly decreased *MYO1D* expression
269 by 8.3-fold (**Fig. 6c,d**). Similarly, CRISPRi-mediated repression of the hub enhancer

270 located in the *SMYD3* SE cluster resulted in more profound downregulation of *SMYD3*
271 expression compared to the non-hub enhancer (**Fig. 6e**).

272 To further interrogate the role of hub versus non-hub enhancers in SE structure
273 and function *in situ*, we employed CRISPR/Cas9-mediated genome engineering to
274 delete individual hub or non-hub enhancers with paired sgRNAs flanking the enhancer
275 elements at the *MYO1D* SE (**Fig. 6f**). We observed that 3 of 5 genes within the SE-
276 containing TAD domain (*MYO1D*, *TMEM98* and *SPACA3*) displayed significant
277 downregulation in mRNA expression, whereas the other two genes (*PSMD11* and
278 *CDK5R1*) remained unaffected (**Fig. 6g** and **Supplementary Fig. 8b**), suggesting that
279 the *MYO1D* SE regulates only a subset of genes within the same TAD domain.
280 Furthermore, knockout of the hub enhancer resulted in more significant downregulation
281 (5.4, 14.0 and 3.2-fold related to control; $P < 0.001$) of *MYO1D*, *TMEM98* and *SPACA3*
282 genes compared to the non-hub enhancers (1.6, 1.5 and 1.5-fold), respectively,
283 consistent with a prominent role of hub enhancers in SE activity. To measure the effects
284 on the local chromatin landscape, we performed ChIP experiments in control, hub and
285 non-hub enhancer knockout cells (**Fig. 6h**). We observed that knockout of the non-hub
286 enhancer had only a subtle effect on the enhancer-associated histone mark (H3K27ac)
287 and binding of master TFs (GATA1 and TAL1) at the promoter or enhancer regions of
288 SE-linked *MYO1D* and *TMEM98* genes. In contrast, knockout of the hub enhancer led to
289 marked downregulation, or near absence, of H3K27ac, H3K4me3 and GATA1/TAL1
290 binding at neighboring enhancers or promoters. These results demonstrate that hub
291 enhancers are functionally more potent than neighboring non-hub enhancers in directing
292 transcriptional activation of SE-linked gene targets.

293 Taken together, our *in situ* genome editing analysis of multiple representative SE
294 clusters provides compelling evidence that at least a subset of SEs are composed of a
295 hierarchical structure containing hub and non-hub enhancer elements, whereby hub
296 enhancers are functionally indispensable for SE activities.

297

298 **Discussion**

299 SE assignment provides a means to identify regulatory regions near important genes
300 that regulate cell fate (Pott & Lieb, 2015). However, it has remained unclear how SEs
301 function and the extent to which they are distinct from more conventional enhancers. As
302 such, the challenge has been to ascribe functional features uniquely associated with
303 SEs, and account for how the activities of the constituent elements are coordinated for

304 SE function(Pott & Lieb, 2015). Here, we have developed a systematic approach to
305 interrogate the structural hierarchy of SE constituent elements. First, we observed that
306 only a subset of SEs contains a hierarchical structure, which is consistent with previous
307 findings that SEs are intrinsically heterogeneous, with a large fraction of SEs containing
308 3 or fewer constituent elements(Pott & Lieb, 2015). Such heterogeneity may provide one
309 explanation for an apparent paradox in the literature(Dukler, Gulko, Huang, & Siepel,
310 2016; Pott & Lieb, 2015). For example, recent studies by our group and others provided
311 evidence that SEs may be composed of a hierarchy of enhancer constituents that
312 coordinately regulate gene expression(Canver et al., 2015; Fulco et al., 2016; Hnisz et
313 al., 2015; Huang et al., 2016; H. Y. Shin et al., 2016). On the other hand, other examples
314 suggest that some SEs may not contain hierarchical structures and the SE constituents
315 contribute additively to gene activation(Hay et al., 2016; Moorthy et al., 2017). Within
316 hierarchical SEs, we identified those hub enhancers associated with an unusually high
317 frequency of long-range chromatin interactions, suggesting that these elements may
318 play an important role in maintaining the structure of SEs. Moreover, hub enhancers are
319 significantly more enriched with eQTL and GWAS-identified genetic variations, and
320 functionally more potent for gene activation than neighboring non-hub enhancers within
321 the same SEs. Hence, our results support a model in which the structural hierarchy of
322 SEs is predictive of functional hierarchy.

323 We observed that CTCF binding is highly enriched at hub enhancers compared
324 to other constituent elements. CTCF has an established role in orchestrating genome
325 structure(Phillips & Corces, 2009). The prevailing model posits that the primary function
326 of CTCF is to maintain the boundaries of topological domains and the insulated
327 neighborhoods(Hnisz, Day, & Young, 2016). Beyond this, our results suggest that CTCF
328 plays additional, yet important, roles in organizing the structural hierarchy of SEs. We
329 speculate that hierarchical organization may be established in a step-wise manner
330 during development through coordinated interactions between CTCF and cell-type
331 specific regulators. Disruption of the hierarchical organization of SE structures may
332 impair SE function and predispose to pathological conditions(Flavahan et al., 2016;
333 Hnisz, Weintraub, et al., 2016; Katainen et al., 2015). Consistent with this model, we
334 found that hub-enhancer-associated CTCF sites display a significantly higher frequency
335 of somatic mutation than non-hub enhancer-associated CTCF sites. Thus, it will be
336 important to investigate chromatin interaction landscapes at both single gene and
337 genomic levels in cancer cells harboring somatic mutations in CTCF sites.

338 At present, Hi-C or ChIA-PET datasets are limited in resolution and available cell
339 types, which presents a significant challenge for further investigation of structural
340 organization within SEs across cell types and cellular conditions. However, the recent
341 development of new technologies, including Hi-ChIP, GAM and capture Hi-C(Beagrie et
342 al., 2017; Mumbach et al., 2016; Schoenfelder et al., 2015), promises to enhance the
343 quality and efficiency of data collection for 3D genome structures in various cell types. At
344 the same time, improved methods for functional validation are also being rapidly
345 developed, such as high-resolution CRISPR/Cas9 mutagenesis(Canver et al., 2017;
346 Canver et al., 2015; Diao et al., 2017). With anticipated availability of additional
347 chromatin interaction datasets, the computational method we describe here should find
348 wide applications to the systematic investigation of the functional and structural
349 organization of regulatory elements, including and beyond SEs. Findings from these
350 studies will provide mechanistic insights into the genetic and epigenetic components of
351 human genome in development and disease.
352

353 **Materials and Methods**

354 **Identification of SEs**

355 ChIP-seq data of H3K27ac in K562 and GM12878 cells were downloaded from
356 ENCODE(T. E. P. Consortium, 2012). All data were in the human genome version hg19.
357 MACS2(Zhang et al., 2008) was used to identify H3K27ac peaks with a threshold Q-
358 value=1.0E-5. H3K27ac peaks were used to define the enhancer boundary, followed by
359 further filtering based on the criteria: (1) excluding H3K27ac peaks that overlapped with
360 ENCODE blacklisted genomic regions(T. E. P. Consortium, 2012); and (2) excluding
361 H3K27ac peaks that were located within +/-2kb region of any Refseq annotated gene
362 promoter. The remaining H3K27ac peaks were defined as enhancers. Then, SEs
363 were identified by using the ROSE (Rank Ordering of Super-Enhancers)
364 algorithm(Loven et al., 2013; Whyte et al., 2013) based on the H3K27ac ChIP-seq signal
365 with the default parameters.

366

367 **Analysis of Hi-C data**

368 The 5kb resolution intra-chromosomal raw interaction matrix in K562 and GM12878 cells
369 were downloaded from a public dataset(Rao et al., 2014). The statistically significant
370 chromatin interactions were detected as previous(Huang et al., 2015). Briefly, the raw
371 interaction matrix was normalized by using the ICE algorithm(Imakaev et al., 2012), as
372 implemented in the Hi-Corrector package(Li, Gong, Li, Alber, & Zhou, 2015), to remove
373 biases(Imakaev et al., 2012; Peng et al., 2013). Fit-Hi-C(Ay, Bailey, & Noble, 2014) was
374 used to identify statistically significant intra-chromosomal interactions, using the
375 parameter setting '-U=2000000, -L=10000' along with the threshold of FDR=0.01. The
376 interaction frequency for each 5kb bin was calculated as the number of significant
377 chromatin interactions associated with the bin. The list of TADs in K562 and GM12878
378 cells were downloaded from the supplementary data(Rao et al., 2014).

379

380 **Analysis of chromatin mark distributions**

381 ChIP-seq of histone marks (H3K27ac, H3K4me1) and transcription factors/co-activators
382 (GATA1, TAL1, PAX5, EBF1, p300, CTCF, SMC3, RAD21), DNase-seq in K562,
383 GM12878 cells were downloaded from ENCODE(T. E. P. Consortium, 2012). Replicate
384 data were merged if available. The sitepro plots for chromatin marks were plotted based
385 on the binned density matrix range from +/-5kb centered by enhancer generated by
386 using the CEAS software(H. Shin, Liu, Manrai, & Liu, 2009).

387

388 **Analysis of CTCF related datasets**

389 Genome-wide CTCF peak locations in 55 cell types, including K562 and GM12878 cells,
390 were downloaded from ENCODE(T. E. P. Consortium, 2012). For each CTCF peak in
391 K562 or GM12878, the cell type consensus score was defined as the percentage of cell
392 types in which the peak was detected.

393 CTCF motif information, represented as a position weight matrix, was
394 downloaded from the JASPAR database(Mathelier et al., 2014). For each CTCF peak
395 in K562 or GM12878, the corresponding maximum motif-matching score was evaluated
396 by using the HOMER software (Heinz et al., 2010).

397 The phastCons scores(Siepel et al., 2005) for multiple alignments of 99
398 vertebrate genomes to the human genome were downloaded from the UCSC Genome
399 Browser. The sitepro plots of conservation score were plotted within +/-200bp centered
400 by CTCF motif sites.

401 Known somatic mutation loci in cancer were downloaded from International
402 Cancer Genome Consortium (ICGC)(International Cancer Genome et al., 2010) Data
403 Portal under release 23. The sitepro plots of mutation frequencies were plotted within +/-
404 200bp centered by CTCF motif sites with a 10bp smoothing window.

405

406 **Enrichment analysis of GWAS SNPs and eQTLs**

407 The SNPs curated in GWAS Catalog(Welter et al., 2014) were downloaded through the
408 UCSC Table Browser(Karolchik et al., 2004). The subset of blood-associated GWAS
409 SNPs was selected as those associated with at least one of the following keywords in
410 the "trait" field: 'Erythrocyte', 'F-cell', 'HbA2', 'Hematocrit', 'Hematological', 'Hematology',
411 'Hemoglobin', 'Platelet', 'Blood', 'Anemia', 'sickle cell disease', 'Thalassemia', 'Leukemia',
412 'Lymphoma', 'Lymphocyte', 'B cell ', 'B-cell', 'Lymphoma', 'Lymphocyte', and 'White blood
413 cell'. Enrichment analysis was carried out as described previously(Huang et al., 2015),
414 using random permutation as control.

415 Statistically significant eQTL loci in multiple tissues were downloaded from the
416 Genotype-Tissue Expression (GTEx) database (Accession phs000424.v6.p1)(G. T.
417 Consortium, 2013). Blood-associated eQTLs were those identified in the whole blood.

418

419 **Analysis of ChIA-PET dataset**

420 CTCF-mediated ChIA-PET data were downloaded from ENCODE (for K562) and from
421 the publication website(Tang et al., 2015) (for GM12878), respectively. The interaction
422 frequency of each 5kb bin was calculated as the number of chromatin interactions
423 associated the PET clusters located in the bin.

424

425 **Data visualization**

426 The ChIP-seq signal and peaks were visualized using Integrative Genomics Viewer
427 (IGV)(Robinson et al., 2011).

428

429 **Cell culture**

430 K562 cells were obtained from the American Tissue Collection Center (ATCC). K562
431 cells were cultured in RPMI1640 medium supplemented with 10% FBS and 1%
432 penicillin-streptomycin.

433

434 **CRISPR/Cas9-Mediated Interference (CRISPRi) of enhancer elements**

435 The CRISPR interference (CRISPRi) system was used to investigate the function of
436 enhancer elements following published protocol with modifications(Gilbert et al., 2014;
437 Thakore et al., 2015). Briefly, sequence-specific sgRNAs for site-specific interference of
438 genomic targets were designed following described guidelines, and sequences were
439 selected to minimize off-target effect based on publicly available filtering tools
440 (<http://crispr.mit.edu/>). Oligonucleotides were annealed in the following reaction: 10 μ M
441 guide sequence oligo, 10 μ M reverse complement oligo, T4 ligation buffer (1X), and 5U
442 of T4 polynucleotide kinase (New England Biolabs) with the cycling parameters of 37°C
443 for 30 min; 95°C for 5 min and then ramp down to 25°C at 5°C/min. The annealed oligos
444 were cloned into pLV-hU6-sgRNA-hUbc-dCas9-KRAB-T2a-Puro vector (Addgene ID:
445 71236) using a Golden Gate Assembly strategy including: 100 ng of circular pLV
446 plasmid, 0.2 μ M annealed oligos, 2.1 buffer (1X) (New England Biolabs), 20 U of BsmBI
447 restriction enzyme, 0.2 mM ATP, 0.1 mg/ml BSA, and 750 U of T4 DNA ligase (New
448 England Biolabs) with the cycling parameters of 20 cycles of 37°C for 5 min, 20°C for 5
449 min; followed by 80°C incubation for 20 min. Then K562 cells were transduced with
450 lentivirus to stably express dCas9-KRAB and sgRNA. To produce lentivirus, we plated
451 K562 cells at a density of 3.0×10^6 per 10 cm plate in high-glucose DMEM
452 supplemented with 10% FBS and 1% penicillin-streptomycin. The next day after
453 seeding, cells were cotransfected with the appropriate dCas9-KRAB lentiviral expression

454 plasmid, psPAX2 and pMD2.G by PEI (Polyethyleneimine). After 8 h, the transfection
455 medium was replaced with 5 mL of fresh medium. Lentivirus was collected 48 h after the
456 first media change. Residual K562 cells were cleared from the lentiviral supernatant by
457 filtration through 0.45 μm cellulose acetate filters. To facilitate transduction, we added
458 the PGE2 (Prostaglandin E2) to the viral media at a concentration of 5 μM . The day after
459 transduction, the medium was changed to remove the virus, and 1 $\mu\text{g}/\text{ml}$ puromycin was
460 used to initiate selection for transduced cells. The positive cells were expanded and
461 processed for gene expression analysis.

462

463 **CRISPR/Cas9-mediated knockout of enhancer elements**

464 The CRISPR/Cas9 system was used to introduce deletion mutations of enhancer
465 elements in K562 cells following published protocols (Canver et al., 2014; Cong et al.,
466 2013; Mali et al., 2013). Briefly, the annealed oligos were cloned into pSpCas9(BB)
467 (pX458; Addgene ID: 48138) vector using a Golden Gate Assembly strategy. To induce
468 segmental deletions of candidate regulatory DNA regions, four CRISPR/Cas9 constructs
469 were co-transfected into K562 cells by nucleofection using the ECM 830 Square Wave
470 Electroporation System (Harvard Apparatus, Holliston, MA). Each construct was directed
471 to flanking the target genomic regions. To enrich for deletion, the top 1-5% of GFP-
472 positive cells were FACS sorted 48-72 h post-transfection and plated in 96-well plates.
473 Single cell derived clones were isolated and screened for CRISPR-mediated deletion of
474 target genomic sequences. PCR amplicons were subcloned and analyzed by Sanger
475 DNA sequencing to confirm non-homologous end-joining (NHEJ)-mediated repair upon
476 double-strand break (DSB) formation. The positive single-cell-derived clones containing
477 the site-specific deletion of the targeted sequences were expanded for processed for
478 gene expression analysis. The sequences of sgRNAs and genotyping PCR primers are
479 listed in Supplementary Table 1.

480

481 **Chromatin immunoprecipitation (ChIP)**

482 ChIP experiments were performed as described with modifications(Huang et al., 2016).
483 Briefly, $2\sim 5 \times 10^6$ cells were crosslinked with 1% formaldehyde for 5 min at room
484 temperature. Chromatin was sonicated to around 500 bp in RIPA buffer (10 mM Tris-
485 HCl, 1 mM EDTA, 0.1% sodium deoxycholate, 0.1% SDS, 1% Triton X-100, 0.25%
486 sarkosyl, pH 8.0) with 0.3 M NaCl. Sonicated chromatin were incubated with 2 μg
487 antibody at 4°C. After overnight incubation, protein A or G Dynabeads (Invitrogen) were

488 added to the CHIP reactions and incubated for four additional hours at 4°C to collect the
489 immunoprecipitated chromatin. Subsequently, Dynabeads were washed twice with 1 ml
490 of RIPA buffer, twice with 1 ml of RIPA buffer with 0.3 M NaCl, twice with 1 ml of LiCl
491 buffer (10 mM Tris-HCl, 1 mM EDTA, 0.5% sodium deoxycholate, 0.5% NP-40, 250 mM
492 LiCl, pH 8.0), and twice with 1 ml of TE buffer (10 mM Tris-HCl, 1 mM EDTA, pH 8.0).
493 The chromatin were eluted in SDS elution buffer (1% SDS, 10 mM EDTA, 50 mM Tris-
494 HCl, pH 8.0) followed by reverse crosslinking at 65°C overnight. CHIP DNA were treated
495 with RNaseA (5 µg/ml) and protease K (0.2 mg/ml), and purified using QIAquick Spin
496 Columns (Qiagen). The purified CHIP DNA was quantified by real-time PCR using the iQ
497 SYBR Green Supermix (Bio-Rad). The following antibodies were used: H3K27ac
498 (ab4729, Abcam), H3K4me3 (04-745, Millipore), IgG (12-370, Millipore), GATA1
499 (ab11852, Abcam), TAL1 (sc-12984, Santa Cruz Biotechnology).

500

501 **Competing interests**

502 The authors declare that they have no competing interests.

503

504 **Authors' contributions**

505 J.H., J.X. and G.C.Y. conceived and designed the experiments. J.H. and Y.Z.
506 performed bioinformatic analyses. K.L. and X.L. performed experimental
507 validation. J.H., J.X., G.C.Y., K.L., W.C. and S.H.O. wrote the manuscript. J.X.
508 and G.C.Y. supervised the project.

509

510 **Acknowledgements**

511 This work was supported by NIH/NIDDK grants K01DK093543, R03DK101665 and
512 R01DK111430, by a Cancer Prevention and Research Institute of Texas (CPRIT) New
513 Investigator award (RR140025), by the American Cancer Society (IRG-02-196) award
514 and the Harold C. Simmons Comprehensive Cancer Center at UT Southwestern, and by
515 an American Society of Hematology Scholar Award (to J.X.). G.C.Y.'s research was
516 supported by the NIH/NHLBI grant R01HL119099. We thank Dr. Alan Cantor and
517 members of the Yuan Lab for helpful discussions.

518

519 References

- 520 Ay, F., Bailey, T. L., & Noble, W. S. (2014). Statistical confidence estimation for Hi-C
521 data reveals regulatory chromatin contacts. *Genome Res*, 24(6), 999-1011. doi:
522 10.1101/gr.160374.113
- 523 Banerji, J., Rusconi, S., & Schaffner, W. (1981). Expression of a beta-globin gene is
524 enhanced by remote SV40 DNA sequences. *Cell*, 27(2 Pt 1), 299-308.
- 525 Beagrie, R. A., Scialdone, A., Schueler, M., Kraemer, D. C., Chotalia, M., Xie, S. Q., . . .
526 Pombo, A. (2017). Complex multi-enhancer contacts captured by genome
527 architecture mapping. *Nature*, 543(7646), 519-524. doi:
528 10.1038/nature21411
- 529 Canver, M. C., Bauer, D. E., Dass, A., Yien, Y. Y., Chung, J., Masuda, T., . . . Orkin, S. H.
530 (2014). Characterization of genomic deletion efficiency mediated by
531 clustered regularly interspaced palindromic repeats (CRISPR)/Cas9 nuclease
532 system in mammalian cells. *J Biol Chem*, 289(31), 21312-21324. doi:
533 10.1074/jbc.M114.564625
- 534 Canver, M. C., Lessard, S., Pinello, L., Wu, Y., Ilboudo, Y., Stern, E. N., . . . Orkin, S. H.
535 (2017). Variant-aware saturating mutagenesis using multiple Cas9 nucleases
536 identifies regulatory elements at trait-associated loci. *Nat Genet*, 49(4), 625-
537 634. doi: 10.1038/ng.3793
- 538 Canver, M. C., Smith, E. C., Sher, F., Pinello, L., Sanjana, N. E., Shalem, O., . . . Bauer, D. E.
539 (2015). BCL11A enhancer dissection by Cas9-mediated in situ saturating
540 mutagenesis. *Nature*, 527(7577), 192-197. doi: 10.1038/nature15521
- 541 Cong, L., Ran, F. A., Cox, D., Lin, S., Barretto, R., Habib, N., . . . Zhang, F. (2013).
542 Multiplex genome engineering using CRISPR/Cas systems. *Science*,
543 339(6121), 819-823. doi: 10.1126/science.1231143
- 544 Consortium, G. T. (2013). The Genotype-Tissue Expression (GTEx) project. *Nat Genet*,
545 45(6), 580-585. doi: 10.1038/ng.2653
- 546 Consortium, T. E. P. (2012). An integrated encyclopedia of DNA elements in the
547 human genome. *Nature*, 489(7414), 57-74. doi: 10.1038/nature11247
- 548 Diao, Y., Fang, R., Li, B., Meng, Z., Yu, J., Qiu, Y., . . . Ren, B. (2017). A tiling-deletion-
549 based genetic screen for cis-regulatory element identification in mammalian
550 cells. *Nat Methods*. doi: 10.1038/nmeth.4264
- 551 Dixon, J. R., Jung, I., Selvaraj, S., Shen, Y., Antosiewicz-Bourget, J. E., Lee, A. Y., . . . Ren,
552 B. (2015). Chromatin architecture reorganization during stem cell
553 differentiation. *Nature*, 518(7539), 331-336. doi: 10.1038/nature14222
- 554 Dixon, J. R., Selvaraj, S., Yue, F., Kim, A., Li, Y., Shen, Y., . . . Ren, B. (2012). Topological
555 domains in mammalian genomes identified by analysis of chromatin
556 interactions. *Nature*, 485(7398), 376-380. doi: 10.1038/nature11082
- 557 Downen, J. M., Fan, Z. P., Hnisz, D., Ren, G., Abraham, B. J., Zhang, L. N., . . . Young, R. A.
558 (2014). Control of cell identity genes occurs in insulated neighborhoods in
559 mammalian chromosomes. *Cell*, 159(2), 374-387. doi:
560 10.1016/j.cell.2014.09.030
- 561 Dukler, N., Gulko, B., Huang, Y. F., & Siepel, A. (2016). Is a super-enhancer greater
562 than the sum of its parts? *Nat Genet*, 49(1), 2-3. doi: 10.1038/ng.3759

- 563 Flavahan, W. A., Drier, Y., Liau, B. B., Gillespie, S. M., Venteicher, A. S., Stemmer-
564 Rachamimov, A. O., . . . Bernstein, B. E. (2016). Insulator dysfunction and
565 oncogene activation in IDH mutant gliomas. *Nature*, *529*(7584), 110-114. doi:
566 10.1038/nature16490
- 567 Fulco, C. P., Munschauer, M., Anyoha, R., Munson, G., Grossman, S. R., Perez, E. M., . . .
568 Engreitz, J. M. (2016). Systematic mapping of functional enhancer-promoter
569 connections with CRISPR interference. *Science*, *354*(6313), 769-773. doi:
570 10.1126/science.aag2445
- 571 Fullwood, M. J., Liu, M. H., Pan, Y. F., Liu, J., Xu, H., Mohamed, Y. B., . . . Ruan, Y. (2009).
572 An oestrogen-receptor-alpha-bound human chromatin interactome. *Nature*,
573 *462*(7269), 58-64. doi: 10.1038/nature08497
- 574 Gilbert, L. A., Horlbeck, M. A., Adamson, B., Villalta, J. E., Chen, Y., Whitehead, E. H., . . .
575 Weissman, J. S. (2014). Genome-Scale CRISPR-Mediated Control of Gene
576 Repression and Activation. *Cell*, *159*(3), 647-661. doi:
577 10.1016/j.cell.2014.09.029
- 578 Hay, D., Hughes, J. R., Babbs, C., Davies, J. O., Graham, B. J., Hanssen, L. L., . . . Higgs, D.
579 R. (2016). Genetic dissection of the alpha-globin super-enhancer in vivo. *Nat*
580 *Genet*, *48*(8), 895-903. doi: 10.1038/ng.3605
- 581 Heinz, S., Benner, C., Spann, N., Bertolino, E., Lin, Y. C., Laslo, P., . . . Glass, C. K. (2010).
582 Simple combinations of lineage-determining transcription factors prime cis-
583 regulatory elements required for macrophage and B cell identities. *Mol Cell*,
584 *38*(4), 576-589. doi: 10.1016/j.molcel.2010.05.004
- 585 Hnisz, D., Abraham, B. J., Lee, T. I., Lau, A., Saint-Andre, V., Sigova, A. A., . . . Young, R.
586 A. (2013). Super-enhancers in the control of cell identity and disease. *Cell*,
587 *155*(4), 934-947. doi: 10.1016/j.cell.2013.09.053
- 588 Hnisz, D., Day, D. S., & Young, R. A. (2016). Insulated Neighborhoods: Structural and
589 Functional Units of Mammalian Gene Control. *Cell*, *167*(5), 1188-1200. doi:
590 10.1016/j.cell.2016.10.024
- 591 Hnisz, D., Schuijers, J., Lin, C. Y., Weintraub, A. S., Abraham, B. J., Lee, T. I., . . . Young, R.
592 A. (2015). Convergence of developmental and oncogenic signaling pathways
593 at transcriptional super-enhancers. *Mol Cell*, *58*(2), 362-370. doi:
594 10.1016/j.molcel.2015.02.014
- 595 Hnisz, D., Weintraub, A. S., Day, D. S., Valton, A. L., Bak, R. O., Li, C. H., . . . Young, R. A.
596 (2016). Activation of proto-oncogenes by disruption of chromosome
597 neighborhoods. *Science*, *351*(6280), 1454-1458. doi:
598 10.1126/science.aad9024
- 599 Huang, J., Liu, X., Li, D., Shao, Z., Cao, H., Zhang, Y., . . . Xu, J. (2016). Dynamic Control
600 of Enhancer Repertoires Drives Lineage and Stage-Specific Transcription
601 during Hematopoiesis. *Dev Cell*, *36*(1), 9-23. doi:
602 10.1016/j.devcel.2015.12.014
- 603 Huang, J., Marco, E., Pinello, L., & Yuan, G. C. (2015). Predicting chromatin
604 organization using histone marks. *Genome Biol*, *16*, 162. doi:
605 10.1186/s13059-015-0740-z
- 606 Imakaev, M., Fudenberg, G., McCord, R. P., Naumova, N., Goloborodko, A., Lajoie, B.
607 R., . . . Mirny, L. A. (2012). Iterative correction of Hi-C data reveals hallmarks

- 608 of chromosome organization. *Nat Methods*, 9(10), 999-1003. doi:
609 10.1038/nmeth.2148
- 610 Ing-Simmons, E., Seitan, V. C., Faure, A. J., Flicek, P., Carroll, T., Dekker, J., ...
611 Merckenschlager, M. (2015). Spatial enhancer clustering and regulation of
612 enhancer-proximal genes by cohesin. *Genome Res*, 25(4), 504-513. doi:
613 10.1101/gr.184986.114
- 614 International Cancer Genome, C., Hudson, T. J., Anderson, W., Artez, A., Barker, A. D.,
615 Bell, C., ... Yang, H. (2010). International network of cancer genome projects.
616 *Nature*, 464(7291), 993-998. doi: 10.1038/nature08987
- 617 Javierre, B. M., Burren, O. S., Wilder, S. P., Kreuzhuber, R., Hill, S. M., Sewitz, S., ...
618 Fraser, P. (2016). Lineage-Specific Genome Architecture Links Enhancers and
619 Non-coding Disease Variants to Target Gene Promoters. *Cell*, 167(5), 1369-
620 1384 e1319. doi: 10.1016/j.cell.2016.09.037
- 621 Ji, X., Dadon, D. B., Powell, B. E., Fan, Z. P., Borges-Rivera, D., Shachar, S., ... Young, R.
622 A. (2016). 3D Chromosome Regulatory Landscape of Human Pluripotent
623 Cells. *Cell Stem Cell*, 18(2), 262-275. doi: 10.1016/j.stem.2015.11.007
- 624 Jin, F., Li, Y., Dixon, J. R., Selvaraj, S., Ye, Z., Lee, A. Y., ... Ren, B. (2013). A high-
625 resolution map of the three-dimensional chromatin interactome in human
626 cells. *Nature*, 503(7475), 290-294. doi: 10.1038/nature12644
- 627 Karolchik, D., Hinrichs, A. S., Furey, T. S., Roskin, K. M., Sugnet, C. W., Haussler, D., &
628 Kent, W. J. (2004). The UCSC Table Browser data retrieval tool. *Nucleic Acids
629 Res*, 32(Database issue), D493-496. doi: 10.1093/nar/gkh103
- 630 Katainen, R., Dave, K., Pitkanen, E., Palin, K., Kivioja, T., Valimaki, N., ... Aaltonen, L. A.
631 (2015). CTCF/cohesin-binding sites are frequently mutated in cancer. *Nat
632 Genet*, 47(7), 818-821. doi: 10.1038/ng.3335
- 633 Li, W., Gong, K., Li, Q., Alber, F., & Zhou, X. J. (2015). Hi-Corrector: a fast, scalable and
634 memory-efficient package for normalizing large-scale Hi-C data.
635 *Bioinformatics*, 31(6), 960-962. doi: 10.1093/bioinformatics/btu747
- 636 Lieberman-Aiden, E., van Berkum, N. L., Williams, L., Imakaev, M., Ragozy, T.,
637 Telling, A., ... Dekker, J. (2009). Comprehensive mapping of long-range
638 interactions reveals folding principles of the human genome. *Science*,
639 326(5950), 289-293. doi: 10.1126/science.1181369
- 640 Loven, J., Hoke, H. A., Lin, C. Y., Lau, A., Orlando, D. A., Vakoc, C. R., ... Young, R. A.
641 (2013). Selective inhibition of tumor oncogenes by disruption of super-
642 enhancers. *Cell*, 153(2), 320-334. doi: 10.1016/j.cell.2013.03.036
- 643 Mali, P., Yang, L., Esvelt, K. M., Aach, J., Guell, M., DiCarlo, J. E., ... Church, G. M. (2013).
644 RNA-guided human genome engineering via Cas9. *Science*, 339(6121), 823-
645 826. doi: 10.1126/science.1232033
- 646 Mathelier, A., Zhao, X., Zhang, A. W., Parcy, F., Worsley-Hunt, R., Arenillas, D. J., ...
647 Wasserman, W. W. (2014). JASPAR 2014: an extensively expanded and
648 updated open-access database of transcription factor binding profiles.
649 *Nucleic Acids Res*, 42(Database issue), D142-147. doi: 10.1093/nar/gkt997
- 650 Maurano, M. T., Humbert, R., Rynes, E., Thurman, R. E., Haugen, E., Wang, H., ...
651 Stamatoyannopoulos, J. A. (2012). Systematic localization of common
652 disease-associated variation in regulatory DNA. *Science*, 337(6099), 1190-
653 1195. doi: 10.1126/science.1222794

- 654 McLean, C. Y., Bristor, D., Hiller, M., Clarke, S. L., Schaar, B. T., Lowe, C. B., . . . Bejerano,
655 G. (2010). GREAT improves functional interpretation of cis-regulatory
656 regions. *Nat Biotechnol*, *28*(5), 495-501. doi: 10.1038/nbt.1630
- 657 Moorthy, S. D., Davidson, S., Shchuka, V. M., Singh, G., Malek-Gilani, N., Langroudi,
658 L., . . . Mitchell, J. A. (2017). Enhancers and super-enhancers have an
659 equivalent regulatory role in embryonic stem cells through regulation of
660 single or multiple genes. *Genome Res*, *27*(2), 246-258. doi:
661 10.1101/gr.210930.116
- 662 Mumbach, M. R., Rubin, A. J., Flynn, R. A., Dai, C., Khavari, P. A., Greenleaf, W. J., &
663 Chang, H. Y. (2016). HiChIP: efficient and sensitive analysis of protein-
664 directed genome architecture. *Nat Methods*, *13*(11), 919-922. doi:
665 10.1038/nmeth.3999
- 666 Parker, S. C., Stitzel, M. L., Taylor, D. L., Orozco, J. M., Erdos, M. R., Akiyama, J. A., . . .
667 Authors, N. C. S. P. (2013). Chromatin stretch enhancer states drive cell-
668 specific gene regulation and harbor human disease risk variants. *Proc Natl*
669 *Acad Sci U S A*, *110*(44), 17921-17926. doi: 10.1073/pnas.1317023110
- 670 Peng, C., Fu, L. Y., Dong, P. F., Deng, Z. L., Li, J. X., Wang, X. T., & Zhang, H. Y. (2013).
671 The sequencing bias relaxed characteristics of Hi-C derived data and
672 implications for chromatin 3D modeling. *Nucleic Acids Res*, *41*(19), e183. doi:
673 10.1093/nar/gkt745
- 674 Phillips, J. E., & Corces, V. G. (2009). CTCF: master weaver of the genome. *Cell*, *137*(7),
675 1194-1211. doi: 10.1016/j.cell.2009.06.001
- 676 Pope, B. D., Ryba, T., Dileep, V., Yue, F., Wu, W., Denas, O., . . . Gilbert, D. M. (2014).
677 Topologically associating domains are stable units of replication-timing
678 regulation. *Nature*, *515*(7527), 402-405. doi: 10.1038/nature13986
- 679 Pott, S., & Lieb, J. D. (2015). What are super-enhancers? *Nat Genet*, *47*(1), 8-12. doi:
680 10.1038/ng.3167
- 681 Rao, S. S., Huntley, M. H., Durand, N. C., Stamenova, E. K., Bochkov, I. D., Robinson, J.
682 T., . . . Aiden, E. L. (2014). A 3D map of the human genome at kilobase
683 resolution reveals principles of chromatin looping. *Cell*, *159*(7), 1665-1680.
684 doi: 10.1016/j.cell.2014.11.021
- 685 Robinson, J. T., Thorvaldsdottir, H., Winckler, W., Guttman, M., Lander, E. S., Getz, G.,
686 & Mesirov, J. P. (2011). Integrative genomics viewer. *Nat Biotechnol*, *29*(1),
687 24-26. doi: 10.1038/nbt.1754
- 688 Schmitt, A. D., Hu, M., Jung, I., Xu, Z., Qiu, Y., Tan, C. L., . . . Ren, B. (2016). A
689 Compendium of Chromatin Contact Maps Reveals Spatially Active Regions in
690 the Human Genome. *Cell Rep*, *17*(8), 2042-2059. doi:
691 10.1016/j.celrep.2016.10.061
- 692 Schoenfelder, S., Furlan-Magaril, M., Mifsud, B., Tavares-Cadete, F., Sugar, R., Javierre,
693 B. M., . . . Fraser, P. (2015). The pluripotent regulatory circuitry connecting
694 promoters to their long-range interacting elements. *Genome Res*, *25*(4), 582-
695 597. doi: 10.1101/gr.185272.114
- 696 Shin, H., Liu, T., Manrai, A. K., & Liu, X. S. (2009). CEAS: cis-regulatory element
697 annotation system. *Bioinformatics*, *25*(19), 2605-2606. doi:
698 10.1093/bioinformatics/btp479

- 699 Shin, H. Y., Willi, M., Yoo, K. H., Zeng, X., Wang, C., Metser, G., & Hennighausen, L.
700 (2016). Hierarchy within the mammary STAT5-driven Wap super-enhancer.
701 *Nat Genet*, 48(8), 904-911. doi: 10.1038/ng.3606
- 702 Siepel, A., Bejerano, G., Pedersen, J. S., Hinrichs, A. S., Hou, M., Rosenbloom, K., . . .
703 Haussler, D. (2005). Evolutionarily conserved elements in vertebrate, insect,
704 worm, and yeast genomes. *Genome Res*, 15(8), 1034-1050. doi:
705 10.1101/gr.3715005
- 706 Tang, Z., Luo, O. J., Li, X., Zheng, M., Zhu, J. J., Szalaj, P., . . . Ruan, Y. (2015). CTCF-
707 Mediated Human 3D Genome Architecture Reveals Chromatin Topology for
708 Transcription. *Cell*, 163(7), 1611-1627. doi: 10.1016/j.cell.2015.11.024
- 709 Thakore, P. I., D'Ippolito, A. M., Song, L., Safi, A., Shivakumar, N. K., Kabadi, A. M., . . .
710 Gersbach, C. A. (2015). Highly specific epigenome editing by CRISPR-Cas9
711 repressors for silencing of distal regulatory elements. *Nat Methods*, 12(12),
712 1143-1149. doi: 10.1038/nmeth.3630
- 713 Welter, D., MacArthur, J., Morales, J., Burdett, T., Hall, P., Junkins, H., . . . Parkinson, H.
714 (2014). The NHGRI GWAS Catalog, a curated resource of SNP-trait
715 associations. *Nucleic Acids Res*, 42(Database issue), D1001-1006. doi:
716 10.1093/nar/gkt1229
- 717 Whyte, W. A., Orlando, D. A., Hnisz, D., Abraham, B. J., Lin, C. Y., Kagey, M. H., . . .
718 Young, R. A. (2013). Master transcription factors and mediator establish
719 super-enhancers at key cell identity genes. *Cell*, 153(2), 307-319. doi:
720 10.1016/j.cell.2013.03.035
- 721 Zhang, Y., Liu, T., Meyer, C. A., Eeckhoute, J., Johnson, D. S., Bernstein, B. E., . . . Liu, X. S.
722 (2008). Model-based analysis of ChIP-Seq (MACS). *Genome Biol*, 9(9), R137.
723 doi: 10.1186/gb-2008-9-9-r137
724
725

726 **Figure legends**

727

728 **Figure 1.** Definition of hierarchical SEs and hub enhancers based on Hi-C chromatin
729 interactions.

730 (a) Overview of pipeline.

731 (b) Representative SEs hierarchical (left) and non-hierarchical (right) SEs. For each 5kb
732 bin within SE, the frequency of chromatin interactions (left *y-axis*) of and the z-score
733 (right *y-axis*) are shown. The dashed red line represents the threshold of z-score = 1.5.

734 (c) The proportion of hierarchical and non-hierarchical SEs.

735 (d) The ROSE ranking of hierarchical and non-hierarchical SEs. *P* value is calculated
736 using Wilcoxon rank-sum test. **P* < 0.05; ***P* < 0.01; ****P* < 0.001.

737 (e) GREAT functional analysis of hierarchical and non-hierarchical SEs.

738

739 **Figure 2.** Chromatin landscapes at hub enhancers.

740 (a-f) Spatial distribution of chromatin marks centered by enhancers in three groups in
741 K562 cells, H3K4me1 (a), H3K27ac (b), DNase I hypersensitivity (c), master regulators
742 GATA1 (d) and TAL1 (e), coactivator p300 (f). *P* values are calculated using Student's t-
743 test based on the ChIP-seq signal intensity within 1kb window centered by enhancers.
744 **P* < 0.05; ***P* < 0.01; ****P* < 0.001, n.s. not significant.

745

746 **Figure 3.** CTCF binding at hub enhancers within SEs hierarchy.

747 (a-c) Spatial distribution of two cohesin components SMC3 (a) and RAD21(b), and
748 CTCF (c), centered by enhancers in three groups. *P* values are calculated using
749 Student's t-test based on the ChIP-seq signal intensity of 1kb window centered by
750 enhancers. **P* < 0.05; ***P* < 0.01; ****P* < 0.001, n.s. not significant.

751 (d) Percentage of hub enhancers with (purple) or without (red) overlapping with TAD
752 boundaries collected from(Rao et al., 2014). The CTCF ChIP-seq peaks/motif-sites
753 associated with hub enhancers overlapping with TAD boundaries were excluded for
754 analysis in (e-h).

755 (e) CTCF binding consensus across cell types in different contexts: hub (red), non-hub
756 enhancers (blue) and TAD boundaries (purple). For each CTCF peak in K562, the
757 consensus score (*y-axis*) was quantified as the percentage of cell types containing the
758 same CTCF peak. *P* values are calculated using Student's t test. **P* < 0.05; ***P* < 0.01;
759 ****P* < 0.001, n.s. not significant.

760 (f) CTCF-motif-matching score (y-axis) of CTCF peaks. P values are calculated using
761 Student's t-test. $*P < 0.05$; $**P < 0.01$; $***P < 0.001$, n.s. *not significant*.

762 (g) Sequence conservation around CTCF motif sites. The sitepro plots were centered by
763 CTCF motif sites. P values are calculated using Student's t-test based on the
764 PhastConst100way score (y-axis) within CTCF motif sites. $*P < 0.05$; $**P < 0.01$; $***P <$
765 0.001 , n.s. *not significant*.

766 (h) Somatic mutation rate in cancers collected from IGGC around CTCF motif sites. The
767 sitepro plots were centered by CTCF motif sites with 10bp smoothing window. P values
768 are calculated using Fisher's exact test based on overlap between CTCF motif sites and
769 somatic mutation sites. $*P < 0.05$; $**P < 0.01$; $***P < 0.001$, n.s. *not significant*.

770 (i) Model of the hierarchical organization of SEs containing both hub and non-hub
771 enhancers. Hub enhancers are highly enriched with CTCF and cohesin binding, and
772 functions as an organization hub to coordinate the non-hub enhancers and other distal
773 regulatory elements within and beyond the SE.

774

775 **Figure 4.** Enrichment of genetic variants associated with cell-type-specific gene
776 expression and diseases in hub enhancers.

777 (a-c) Enrichment of the eQTLs curated in GTEx in the enhancers in three groups in
778 K562 cells, using randomly selected genome regions as control (see Methods). The
779 GTEx eQTL identified in all tissues (a) were separated into two subsets, identified in
780 whole blood (b) or other tissues (c). The number of enhancers overlap in each group
781 with eQTLs were labelled on each bar. P values are calculated using Fisher's exact test.
782 $*P < 0.05$; $**P < 0.01$; $***P < 0.001$, n.s. *not significant*.

783 (d-f) Enrichment of the disease or traits-associated SNPs curated in GWAS catalog in
784 the enhancers in three groups in K562 cells, using randomly selected genome regions
785 as control (see Methods). The GWAS SNPs associated all diseases/traits (d), were
786 separated into two subsets, associated with blood-related diseases/traits (e) or other
787 traits (f). The number of enhancers overlap in each group with SNPs were labelled on
788 each bar. P values are calculated using Fisher's exact test. $*P < 0.05$; $**P < 0.01$; $***P <$
789 0.001 , n.s. *not significant*.

790

791 **Figure 5.** *In situ* genome editing reveals distinct requirement of hub vs non-hub
792 enhancers in SE function.

793 **(a)** Chromatin signatures and TF occupancy at the MYO1D SE locus in K562 cells are
794 shown. The identified hub and non-hub enhancers are depicted by red (hub) and blue
795 (non-hub) lines, respectively. The Hi-C chromatin interaction z-score and frequency at
796 5kb resolution is shown at the bottom (see Methods). The positions of sgRNAs used for
797 CRISPRi or CRISPR/Cas9-mediated knockout analyses are shown as arrowheads.
798 **(b)** Chromatin signatures and TF occupancy at the SMYD3 SE locus in K562 cells are
799 shown.
800 **(c)** Schematic of CRISPRi-mediated repression of hub or non-hub enhancers.
801 **(d,e)** Expression of MYO1D and SMYD3 mRNA in untreated (control), CRISPRi-
802 mediated repression of hub or non-hub enhancers. The mRNA expression levels related
803 to GAPDH are shown. Each colored circle represents an independent biological replicate
804 experiment. Results are means \pm SEM. *P* values are calculated by two-sided Student's t-
805 test. **P* < 0.05, ***P* < 0.01, ****P* < 0.001, n.s. not significant.
806 **(f)** Schematic of CRISPR/Cas9-mediated knockout of hub or non-hub enhancers.
807 **(g)** Expression of all genes within the SE-containing TAD domain in unmodified (control),
808 CRISPR/Cas9-mediated knockout of hub or non-hub enhancers. The mRNA expression
809 levels relative to GAPDH are shown. Each colored circle represents an independent
810 single-cell-derived biallelic enhancer knockout clone. A schematic of the SE-containing
811 TAD domain and associated genes are shown on the top. Results are means \pm SEM. *P*
812 values are calculated by a two-sided Student's t-test. **P* < 0.05, ***P* < 0.01, ****P* < 0.001,
813 n.s. not significant.
814 **(h)** ChIP-qPCR analysis of H3K27ac, H3K4me3, GATA1, TAL1 and IgG (negative
815 control) in unmodified (control), hub or non-hub enhancer knockout cells. Primers
816 against MYO1D and TMEM98 promoters, hub and non-hub enhancers, and a negative
817 control genome region (chr2:211,337,339-211,337,429) are used. The results are shown
818 as fold enrichment of the ChIP signals against the negative control region as means \pm
819 SEM of four independent experiments. *P* values are calculated by a two-sided Student's
820 t-test. **P* < 0.05, ***P* < 0.01, ****P* < 0.001, n.s. not significant.
821

822 **Supplementary Figures and Tables**

823

824 **Supplementary Figure 1.** Definition of hierarchical SEs and hub enhancers using
825 chromatin interactions in K562 and GM12878 cells. Related to **Fig. 1**.

826 (a) Chromatin interactions frequency for 5kb bins overlapping with SEs (yellow), REs
827 (green), using randomly selected genome 5kb bins as control (gray) in K562 and
828 GM12878 cells. *P* values are calculated using Student's t-test. **P* < 0.05; ***P* < 0.01;
829 ****P* < 0.001, n.s. not significant.

830 (b) Distribution of z-score of 5kb bins in all SEs. The dashed line represents the
831 threshold value of H-score = 1.5, which roughly corresponds to the 95th percentile of z-
832 scores.

833 (c) Hierarchical SEs and hub enhancers defined using different thresholds of H-score.

834 (d) The frequency of chromatin interaction of enhancers in three groups of enhancers
835 (red for hub enhancers, blue for non-hub enhancers, green for regular enhancers). *P*
836 values are calculated using Student's t-test. **P* < 0.05; ***P* < 0.01; ****P* < 0.001, n.s. not
837 significant.

838

839 **Supplementary Figure 2.** Hierarchical and non-hierarchical SEs in GM12878 cells.
840 Related to **Fig. 1**.

841 (a) Proportion of hierarchical and non-hierarchical SEs.

842 (b) The ROSE ranking of hierarchical and non-hierarchical SEs. *P* value is calculated
843 using Wilcoxon rank-sum test. **P* < 0.05; ***P* < 0.01; ****P* < 0.001, n.s. not significant.

844 (c) GREAT functional analysis of hierarchical and non-hierarchical SEs.

845

846 **Supplementary Figure 3.** Chromatin landscapes around hub enhancers in GM12878
847 cells. Related to **Fig. 2**.

848 (a-f) Spatial distribution of chromatin marks centered by enhancers in three groups,
849 H3K4me1 (a), H3K27ac (b), DNase I hypersensitivity (c), master regulators PAX5 (d)
850 and EBF1 (e), and coactivator p300 (f).

851

852 **Supplementary Figure 4.** CTCF binding at hub enhancers within SEs hierarchy in
853 GM12878 cells. Related to **Fig. 3**.

854 (a-c) Spatial distribution of two cohesin components SMC3, RAD21 (a,b) and CTCF (c),
855 centered by enhancers in three groups.

856 (d) Percentage of hub enhancers with (purple) or without (red) overlapping with TAD
857 boundaries collected from (Rao et al., 2014). The CTCF ChIP-seq peaks/motif-sites
858 associated with hub enhancers overlapping with TAD boundaries were excluded for
859 analysis in (e-h).

860 (e) CTCF binding consensus across cell types in different contexts: hub (red), non-hub
861 enhancers (blue) and TAD boundaries (purple). For each CTCF peak in GM12878, the
862 consensus score (y-axis) was quantified as the percentage of cell types containing the
863 same CTCF peak. P values are calculated using Student's t test. $*P < 0.05$; $**P < 0.01$;
864 $***P < 0.001$, n.s. not significant.

865 (f) CTCF-motif-matching score (y-axis) of CTCF peaks. P values are calculated using
866 Student's t -test. $*P < 0.05$; $**P < 0.01$; $***P < 0.001$, n.s. not significant.

867 (g) Sequence conservation around CTCF motif sites. The sitepro plots were centered by
868 CTCF motif sites. P values are calculated using Student's t -test based on the
869 PhastConst100way score (y-axis) within CTCF motif sites. $*P < 0.05$; $**P < 0.01$; $***P <$
870 0.001 , n.s. not significant.

871 (h) Somatic mutation rate in cancers collected from IGGC around CTCF motif sites. The
872 sitepro plots were centered by CTCF motif sites with 10bp smoothing window. P values
873 are calculated using Fisher's exact test based on overlap between CTCF motif sites and
874 somatic mutation sites. $*P < 0.05$; $**P < 0.01$; $***P < 0.001$, n.s. not significant.

875

876 **Supplementary Figure 5.** Enrichment of genetic variants associated with cell-type
877 specific gene expression and diseases in hub enhancers in GM12878 cells. Related to
878 **Fig. 4.**

879 (a-c) Enrichment of the eQTLs curated in GTEx in the enhancers in three groups, using
880 randomly selected genome regions as control (see Methods). The GTEx eQTL identified
881 in all tissues (a) were separated into two subsets, identified in blood (b) or other tissues
882 (c). The number of enhancers overlap in each group with eQTLs were labelled on each
883 bar. P values are calculated using Fisher's exact test. $*P < 0.05$; $**P < 0.01$; $***P < 0.001$,
884 n.s. not significant.

885 (d-f) Enrichment of the disease or traits-associated SNPs curated in GWAS catalog in
886 the enhancers in three groups, using randomly selected genome regions as control (see
887 Methods). The GWAS SNPs associated all diseases/traits (d), were separated into two
888 subsets, associated with blood-related diseases/traits (e) or other traits (f). The number
889 of enhancers overlap in each group with SNPs were labelled on each bar. P values are

890 calculated using Fisher's exact test. $*P < 0.05$; $**P < 0.01$; $***P < 0.001$, n.s. not
891 significant.

892

893 **Supplementary Figure 6.** Enrichment of genetic variants associated with cell-type
894 specific expression and diseases in K562 and GM12878. Related to **Fig. 4.**

895 (a) Enrichment of GTEx eQTL (left) and GWAS SNPs (right) in SEs and REs in K562
896 (upper) and GM12878(lower). The number of enhancers overlap in each group with
897 eQTLs were labelled on each bar. P values are calculated using Fisher's exact test. $*P <$
898 0.05 ; $**P < 0.01$; $***P < 0.001$, n.s. not significant.

899 (b,c) Enrichment of GTEx eQTL (left) and GWAS SNPs (right) in hub enhancers defined
900 based on the threshold of H-score >1.25 (b) or H-score >1.75 (c) in K562 (upper) and
901 GM12878(lower). The number of enhancers overlap in each group with eQTLs were
902 labelled on each bar. P values are calculated using Fisher's exact test. $*P < 0.05$; $**P <$
903 0.01 ; $***P < 0.001$, n.s. not significant.

904

905 **Supplementary Figure 7.** Comparison of hub enhancers defined based on chromatin
906 interactions from Hi-C and ChIA-PET datasets in K562 and GM12878 cells. Related to
907 **Fig. 5.**

908 (a) Overlap between hierarchical SEs (left) or hub enhancers (right) using Hi-C and
909 ChIA-PET dataset in K562 (upper) and GM12878 (lower). P values are calculated using
910 Fisher's exact test. $*P < 0.05$; $**P < 0.01$; $***P < 0.001$, n.s. not significant.

911 (b) Enrichment of GTEx eQTL (left) or GWAS SNPs (right) in hub enhancers defined
912 based on ChIA-PET. P values are calculated using Fisher's exact test. $*P < 0.05$; $**P <$
913 0.01 ; $***P < 0.001$, n.s. not significant.

914

915 **Supplementary Figure 8.** *In situ* analysis of the functional requirement of hub vs non-
916 hub enhancers. Related to **Fig. 6.**

917 (a) A genome browser view of the chromatin signatures and TF occupancy at the
918 SLC25A37 SE locus in K562 cells. The identified SE is depicted by the blue shaded area.
919 The hub and non-hub enhancers are denoted by the red and blue shaded lines,
920 respectively. The Hi-C chromatin interaction z-score and frequency at 5kb resolution is
921 shown at the bottom (see Methods).

922 (b) A zoom-out view of the chromatin signatures and TF occupancy at the MYO1D SE
923 locus in K562 cells is shown.

924 (c) A zoom-out view of the chromatin signatures and TF occupancy at the SMYD3 SE
925 locus in K562 cells is shown.

926

927 **Supplementary Table 1.** List of primer and sgRNA sequences used in this study,
928 Related to the **Fig. 5** and **Supplementary Fig. 8.**

929

Figure 1

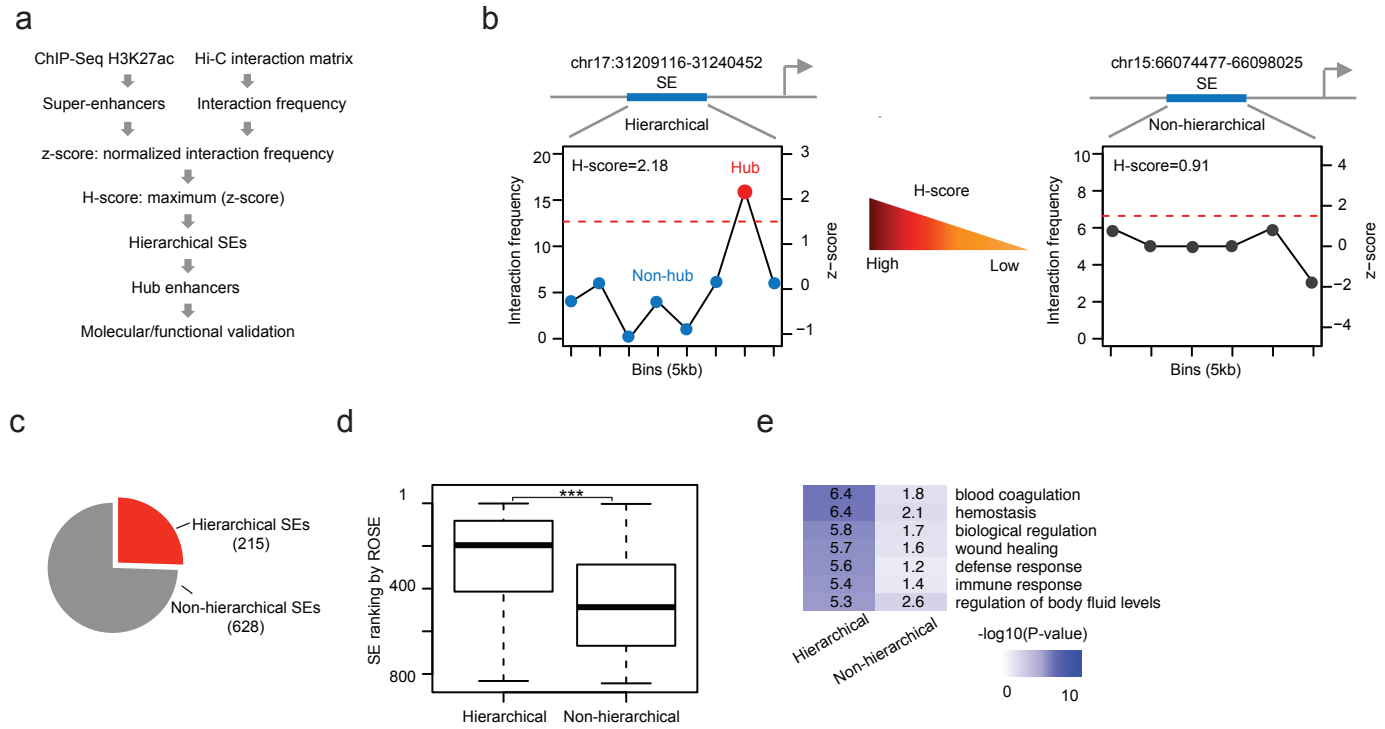


Figure 2

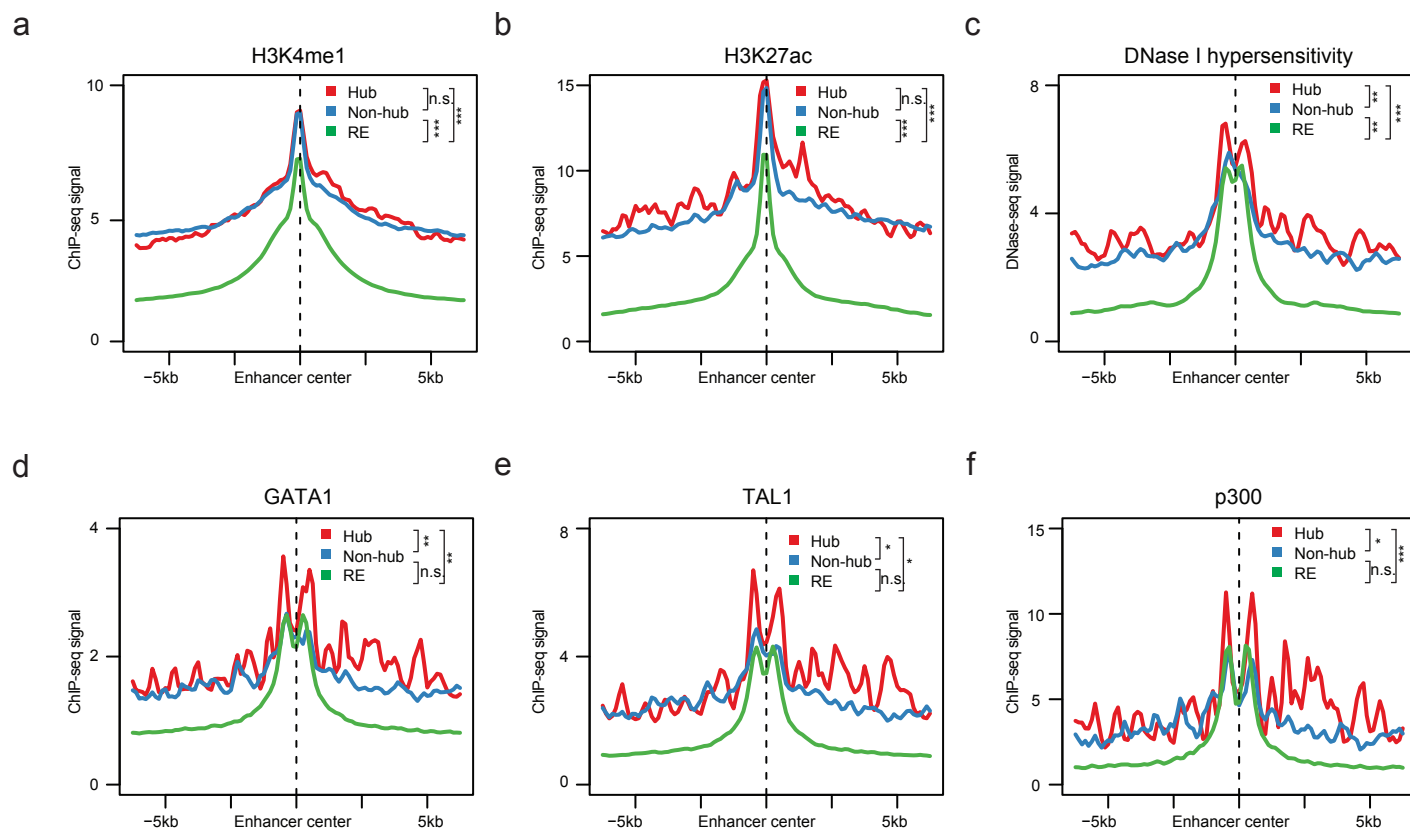


Figure 3

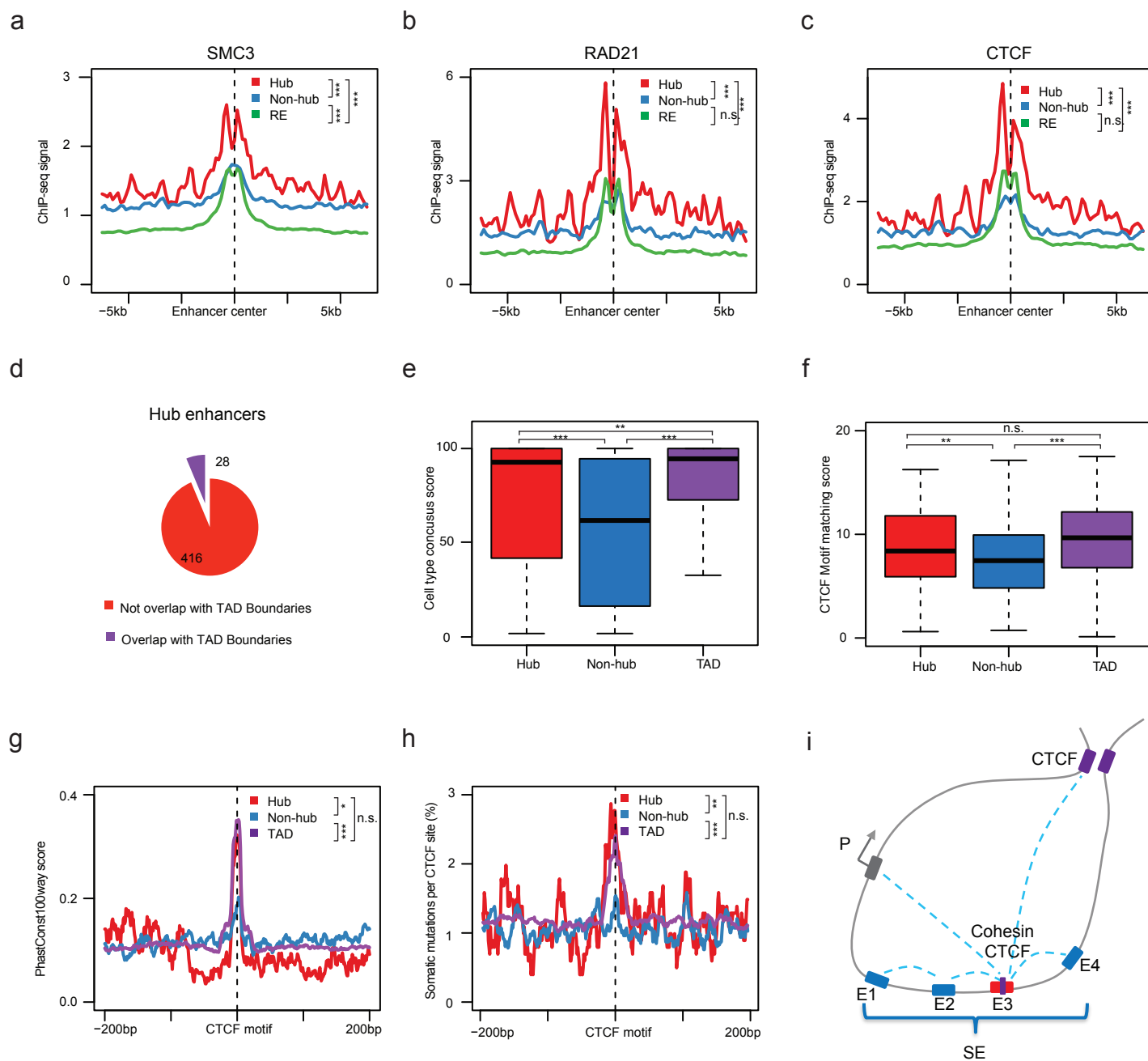


Figure 4

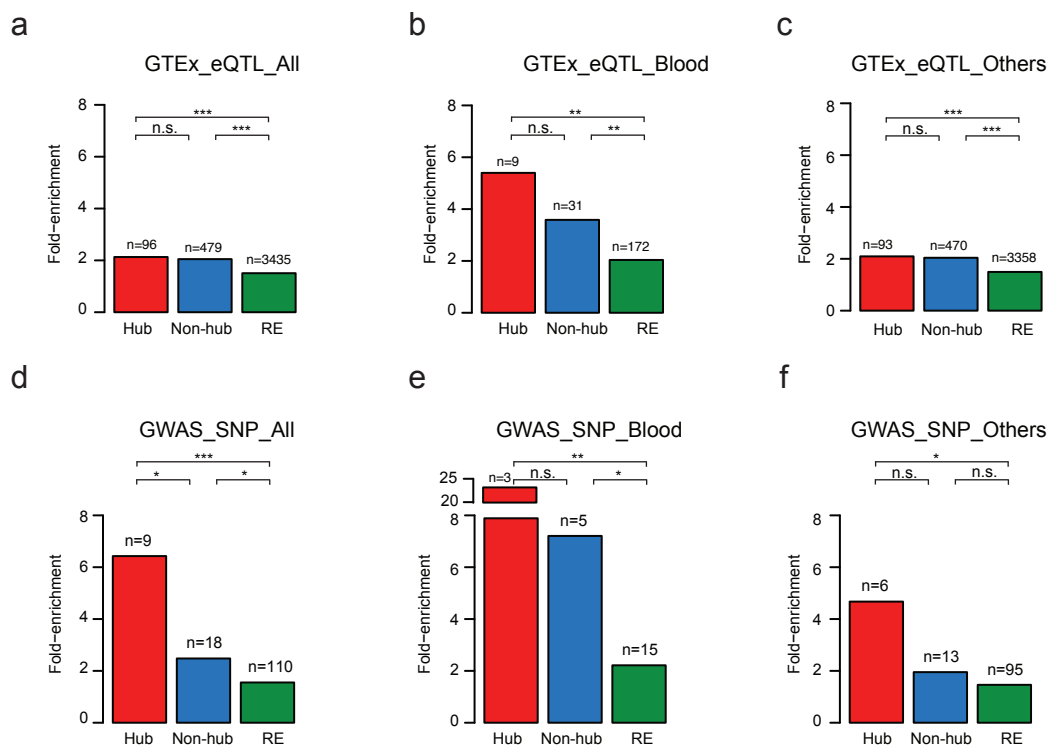
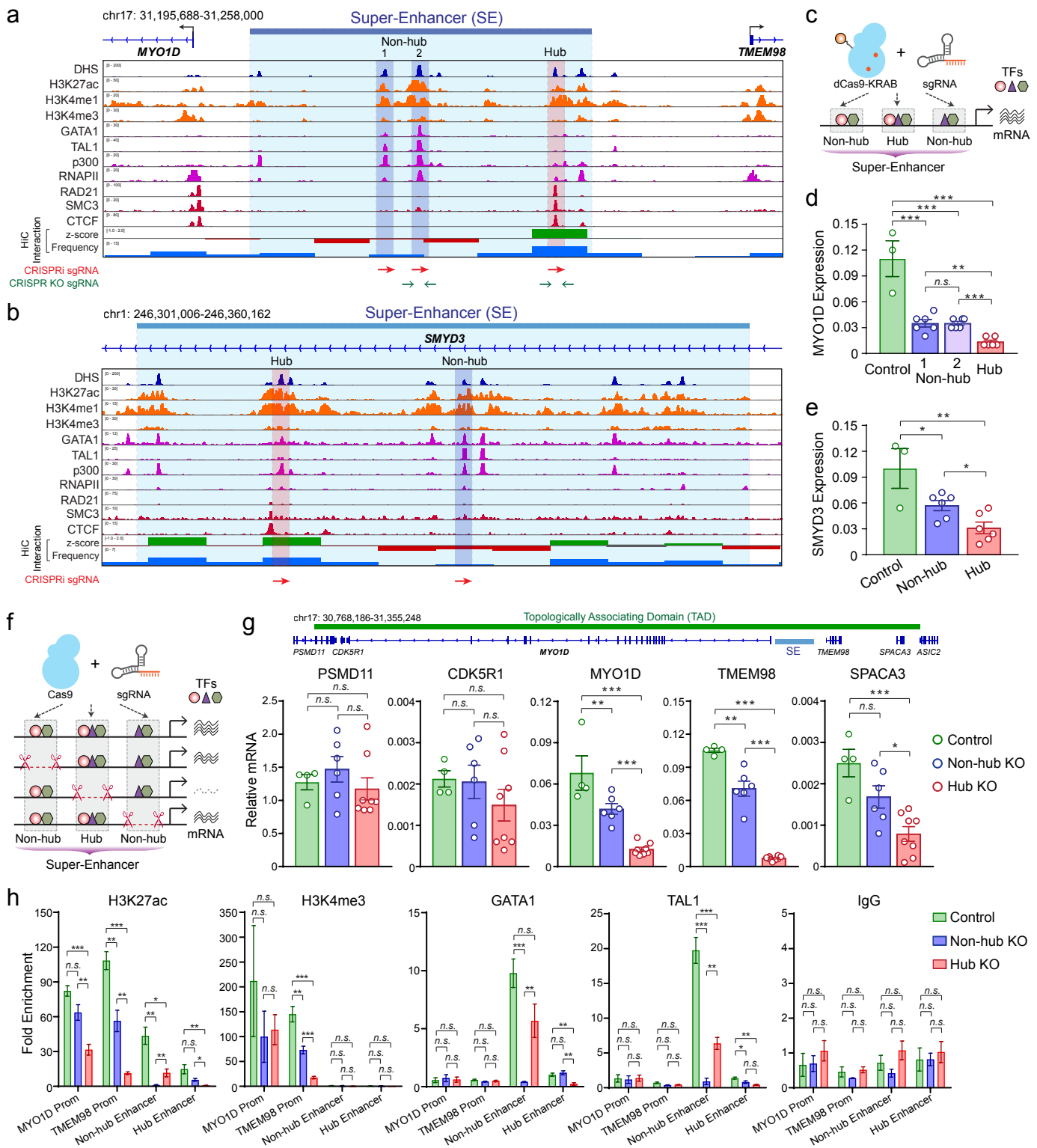
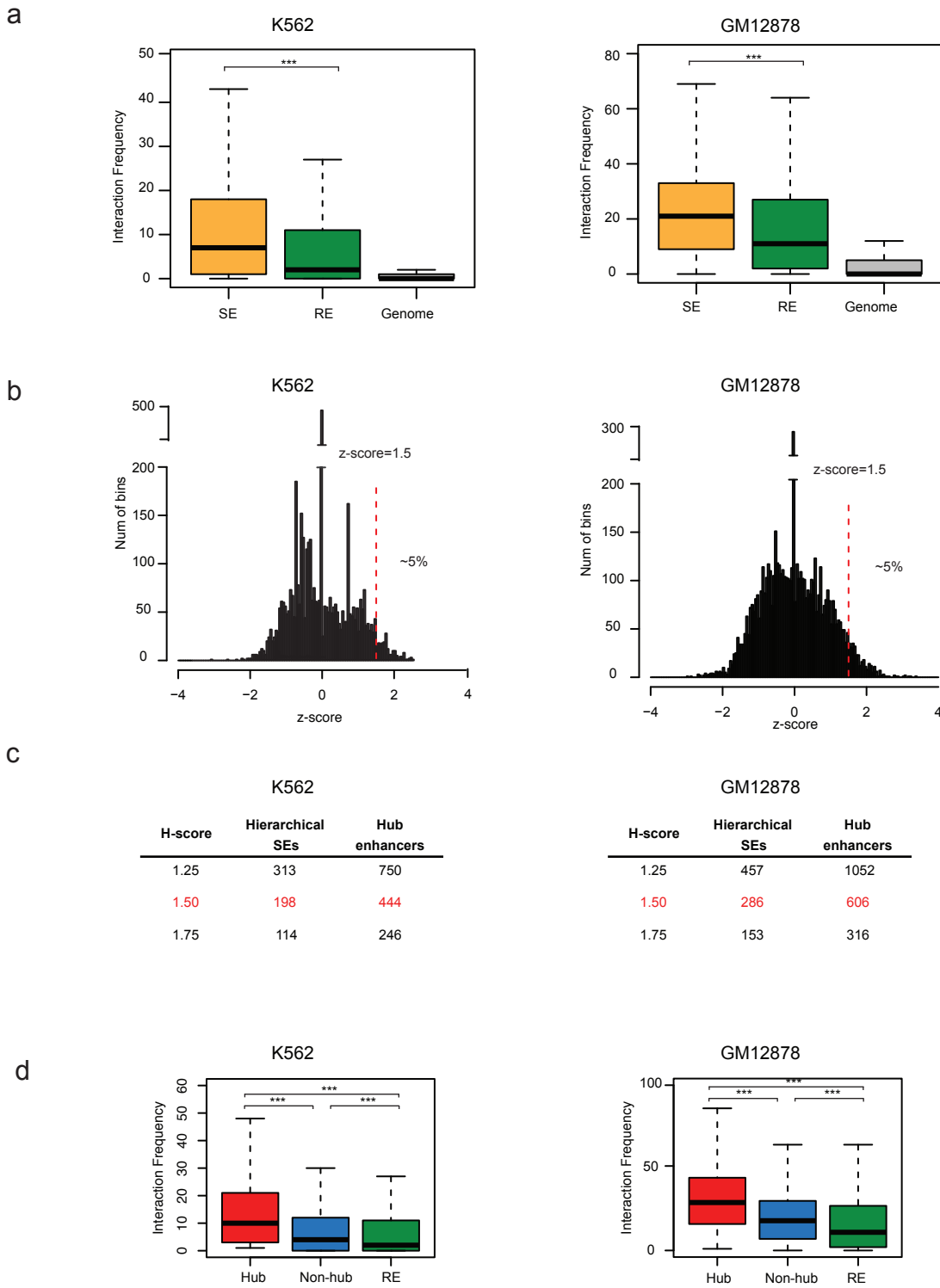


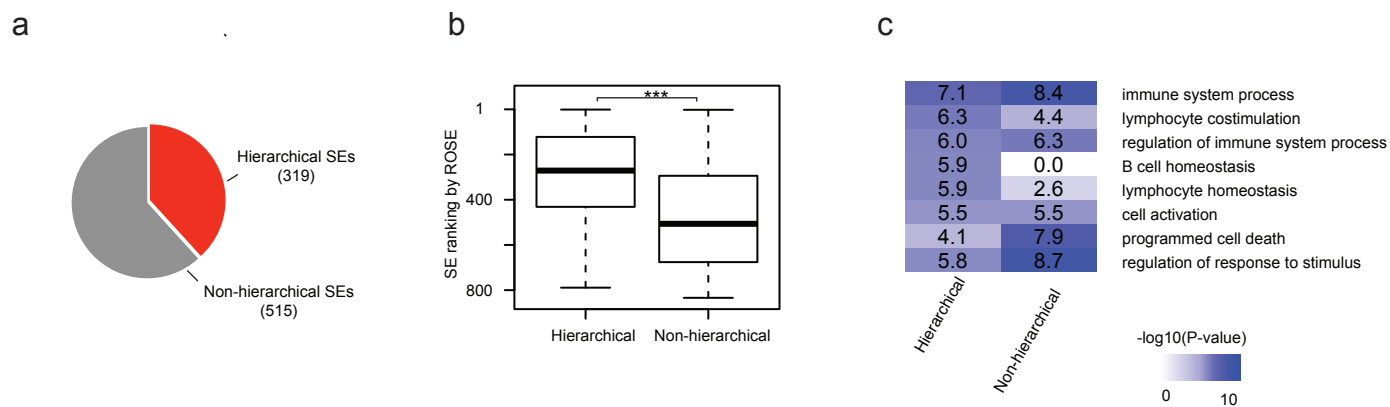
Figure 5



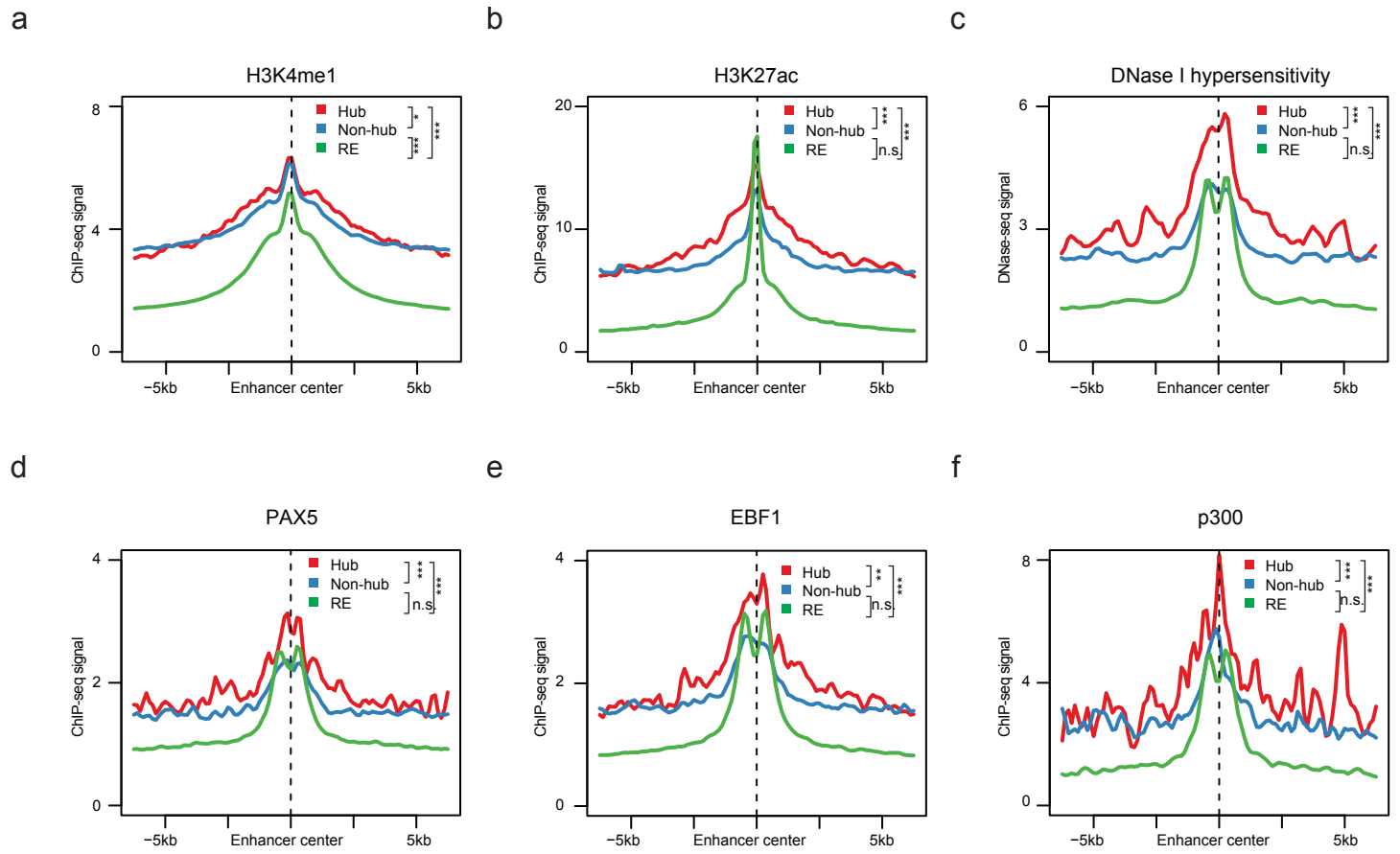
Supplementary Figure 1



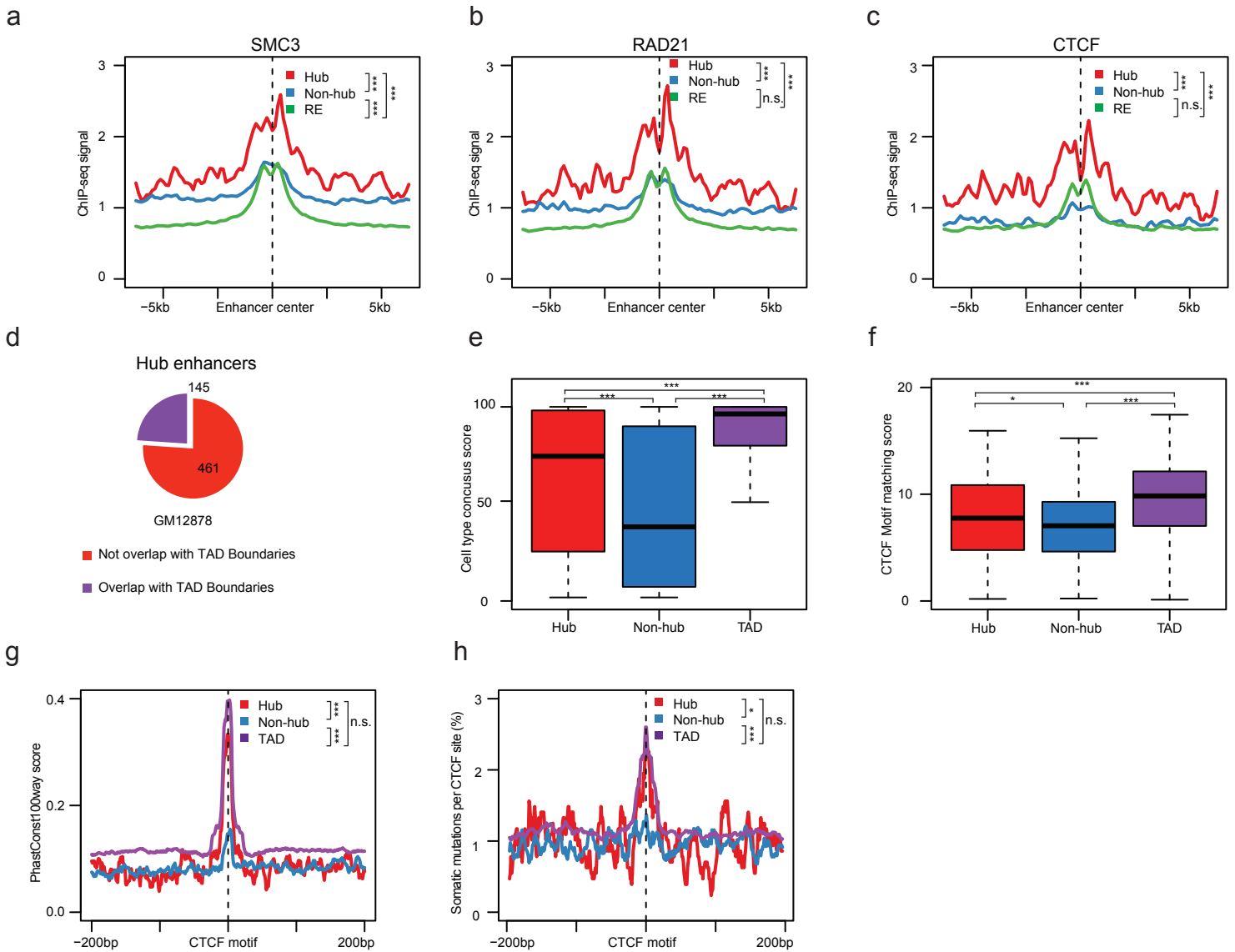
Supplementary Figure 2



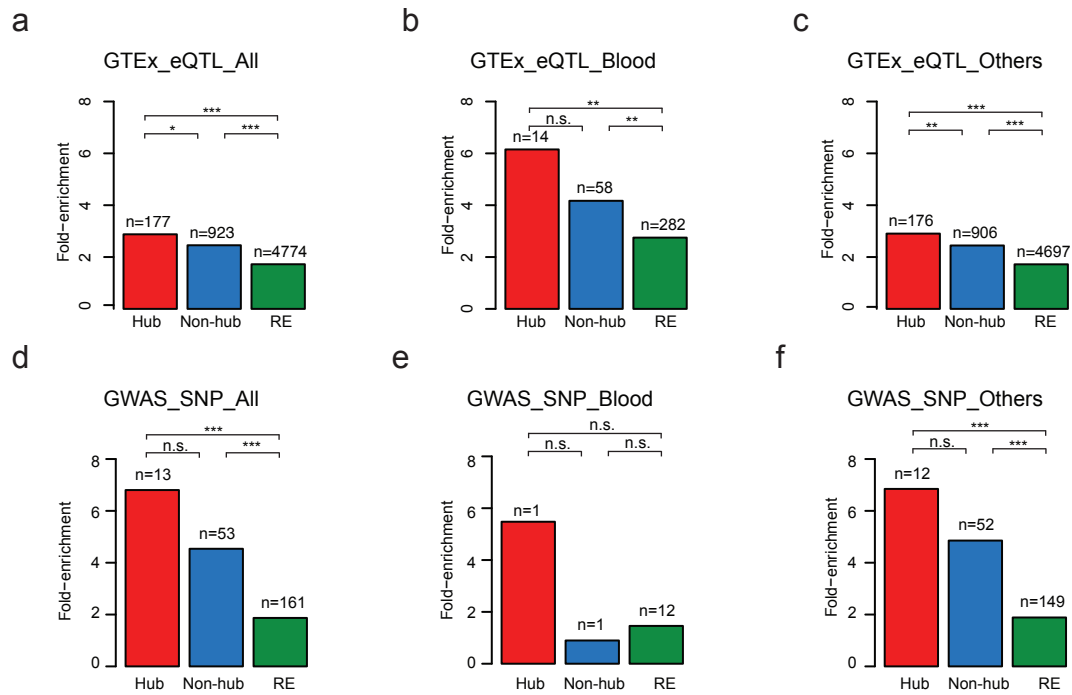
Supplementary Figure 3



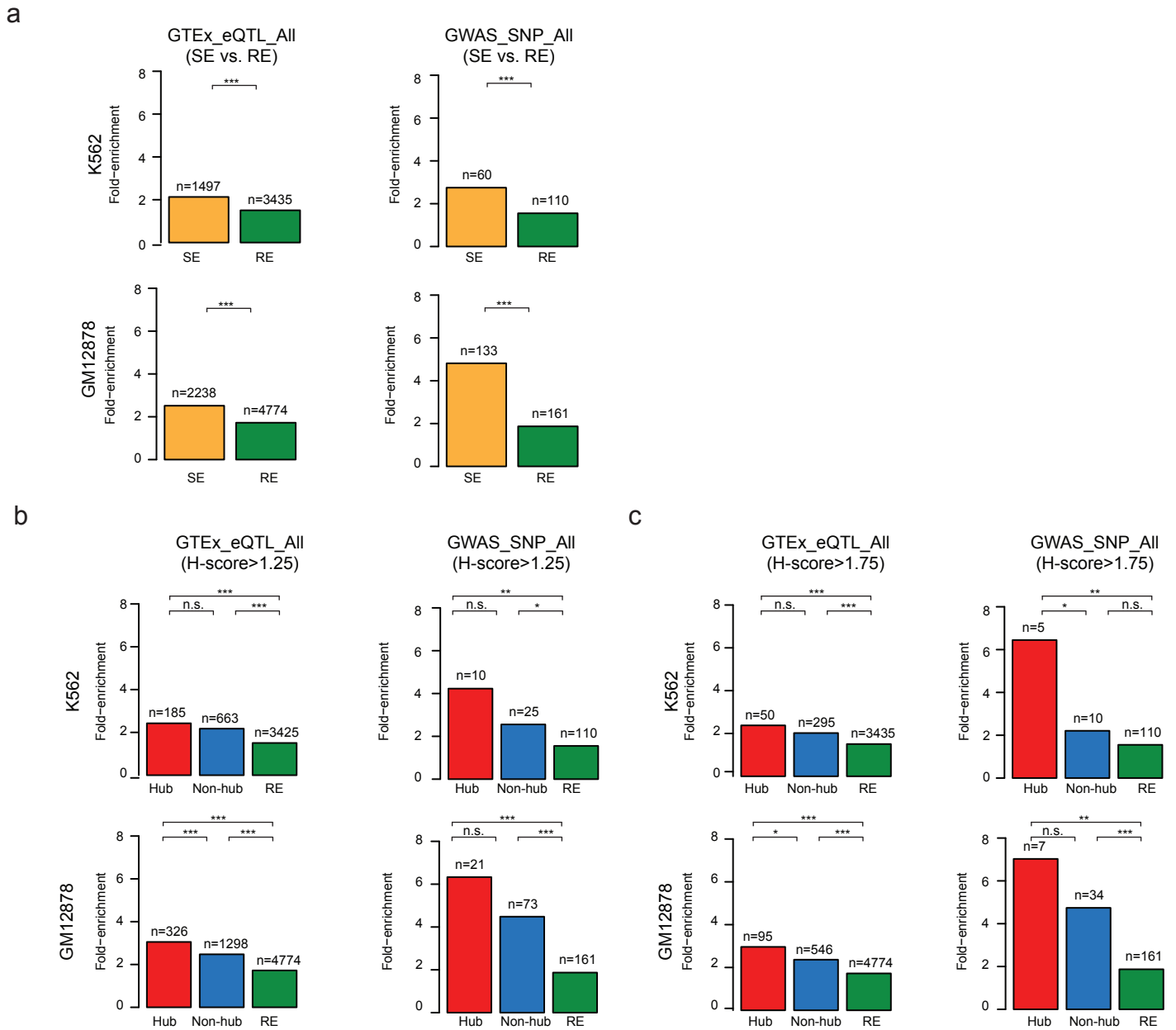
Supplementary Figure 4



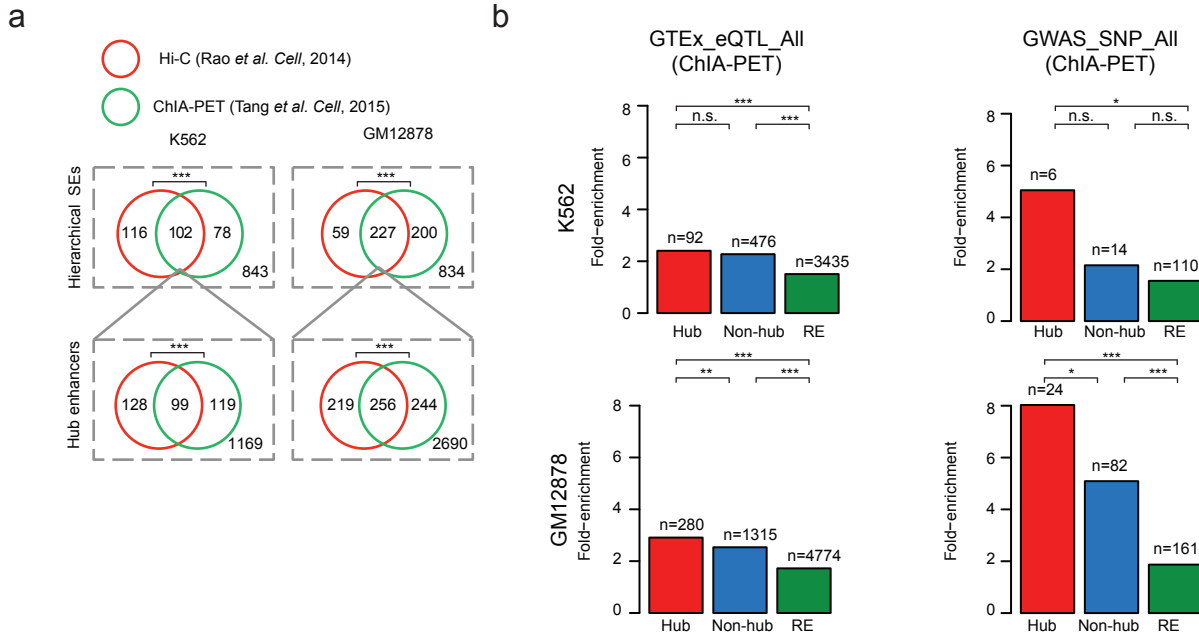
Supplementary Figure 5



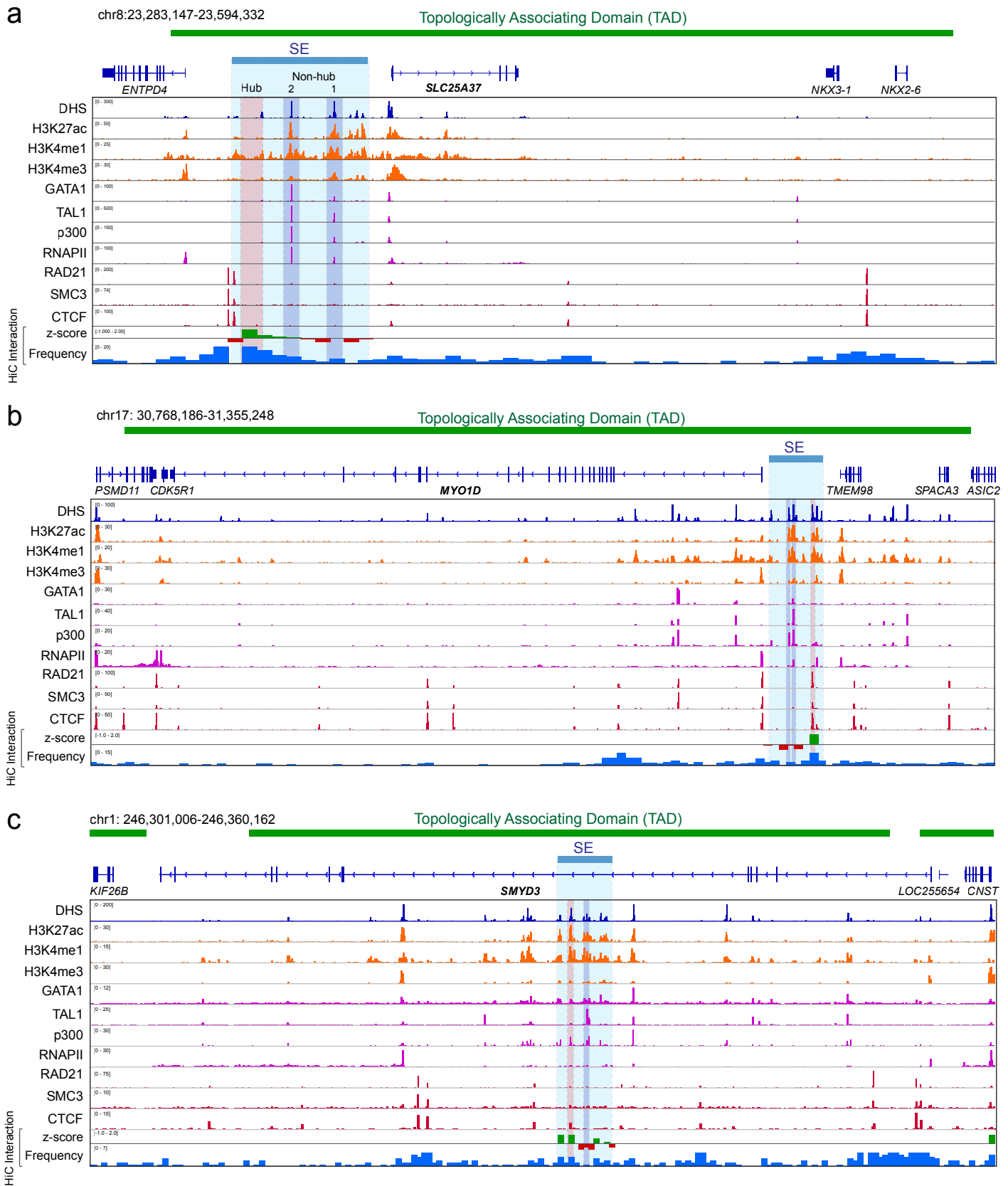
Supplementary Figure 6



Supplementary Figure 7



Supplementary Figure 8



Supplementary Table 1. List of primer and sgRNA sequences used in this study, Related to the **Fig. 5** and **Supplementary Fig. 8.**

<i>Name</i>	<i>Forward</i>	<i>Reverse</i>	<i>Application</i>
MYO1D_Non-hub Enh1-sgRNA1	CACCGCTTATCTGTTCTGTTCTGTC	AAACGACACGAACGAACAGATAAGC	sgRNA oligos for CRISPRi
MYO1D_Non-hub Enh1-sgRNA2	CACCGTGAAGTATGACTAATTGC	AAACGCAATTAGTGTATCAGTTCAC	
MYO1D_Non-hub Enh2-sgRNA1	CACCGCATGTAGCAACATGTGATAC	AAACGTATCACATGTTGCTACATGC	
MYO1D_Non-hub Enh2-sgRNA2	CACCGCATTGGCACTCTCTGCCGTC	AAACGACGGCAGAGAGTGCCAATGC	
MYO1D_Hub Enh-sgRNA1	CACCGGTAACGTTGAAGATTGCTG	AAACGAGCAATCTTCAACGTTAGCC	
MYO1D_Hub Enh-sgRNA2	CACCGGCACTTCAAAGAGTGGTCAC	AAACGTGACCACTCTTTGAAGTGCC	
SMYD3_Hub Enh-sgRNA1	CACCGGGACTGTTCTCTCAAAAAGT	AAACACTTTTGAGAGGAACAGTCCC	
SMYD3_Hub Enh-sgRNA2	CACCGGAAGTCCAGTTATGACTGT	AAACACAGTCATAACCTGGACTTCC	
SMYD3_Non-hub Enh-sgRNA1	CACCGGTGAGCTTACCCGTGACTCC	AAACGGAGTCACGGGTAAGCTCACC	
SMYD3_Non-hub Enh-sgRNA2	CACCGCTATCTATTCGTTGCAGTG	AAACCACTGCAACGAATAGATAGGC	
Gal4-4 sgRNA	CACCGAACGACTAGTTAGGCGTGTA	AAACTACACGCCCTAACTAGTCGTTTC	
MYO1D_Non-hub Enh2-sgRNA1	CACCGCTTAGGAGGGGTAGGCACCC	AAACGGGTGCCTACCCCTCCTAAGC	
MYO1D_Non-hub Enh2-sgRNA2	CACCGCACCCCGTGCATAAGAAAT	AAACATTTCTTATGCCACGGGGTGC	
MYO1D_Non-hub Enh2-sgRNA3	CACCGTAGTGATTTGGGGGTCCCA	AAACTGGGACCCCAAAATCACTAC	
MYO1D_Non-hub Enh2-sgRNA4	CACCGGAGAAAATAATCTGCTCTC	AAACGAGAGCAGATTAATTTTCTCC	
MYO1D_Hub Enh-sgRNA1	CACCGGAGATGAGATACAGAGTAG	AAACCTACTCTGTATCTCATCTCCC	
MYO1D_Hub Enh-sgRNA2	CACCGGTAAAGCAGAATAGGGGCAT	AAACATGCCCTATTCTGCTTTACC	
MYO1D_Hub Enh-sgRNA3	CACCGCCATTTTACAGTTGTCCCCC	AAACGGGGGACAACGTAAAATGGC	
MYO1D_Hub Enh-sgRNA4	CACCGTCTCATTCTCGTCGCCAC	AAACGTGGCAGCAAGGAATGAGAC	
MYO1D_Non-hub Enh2-del	ATAGGGTCTCACTACGTTTCCCAGG	CCCTACGAACCTGAAACTAGACAAC	genotyping primers for enhancer KO
MYO1D_Non-hub Enh2-WT	ATAGGGTCTCACTACGTTTCCCAGG	TCCTACACATCATGCACCTTCTC	
MYO1D_Hub Enh-del	AAGTTGAAGAGAGAACGGGAGGTAG	CCCTGGCTCTGTTGTGAAATGTGG	
MYO1D_Hub Enh-WT	AAGTTGAAGAGAGAACGGGAGGTAG	CACGGAGTTGCTCTCTTCTCTTC	RT-qPCR primers
hMYO1D_RT	AAGGCAGACTTCGTGCTGATG	TAAGGGTTCACAGAAACGACG	
hTMEM98_RT	TTCTGGCTTCGTTTGACGC	CGTCCAGTTCTAACTCAGAGGG	
hSPACA3_RT	CCGGCATAGAAGCCAGGAG	TCACAACGACCCGTAGAGCTTG	
hCDK5R1_RT	AGAACAGCAAGAACGCCAAG	CGGCCACGATTCTCTTCCA	
hPSMD11_RT	GCCTCCATCGACATCCTCC	GAGCTGCTTTAGCCTTGCTG	
hSMYD3_RT	CGCGTCGCCAAATACTGTAGT	CAAGAAGTCGAACGGAGTCTG	
hGAPDH_RT	ACCCAGAAGACTGTGGATGG	TTCAGCTCAGGGATGACCTT	
MYO1D_Non-hub Enh2	GGACACATCCGAGGAAGACCAAG	GACATTTCTCAATCTTCAGCCTCTC	ChIP-qPCR primers
MYO1D_Hub Enh	TTTAGAAGCAGTGGTACACCCAG	GAGAATGGTGAGGGCTCTGATGC	
MYO1D Prom	TCTCGGGAAGCGCAGCCTC	GGCAAGGCAGACTTCGTGCTGATG	
TMEM98 Prom	GCGGGTGCCGACGTTTGTCTTG	GACCCAAGACCTACCCGCTTC	
Ctrl	AAACCCACGTCCAGCACAGTGTG	AATAGCGGGTAAGGATGTAGACAGG	